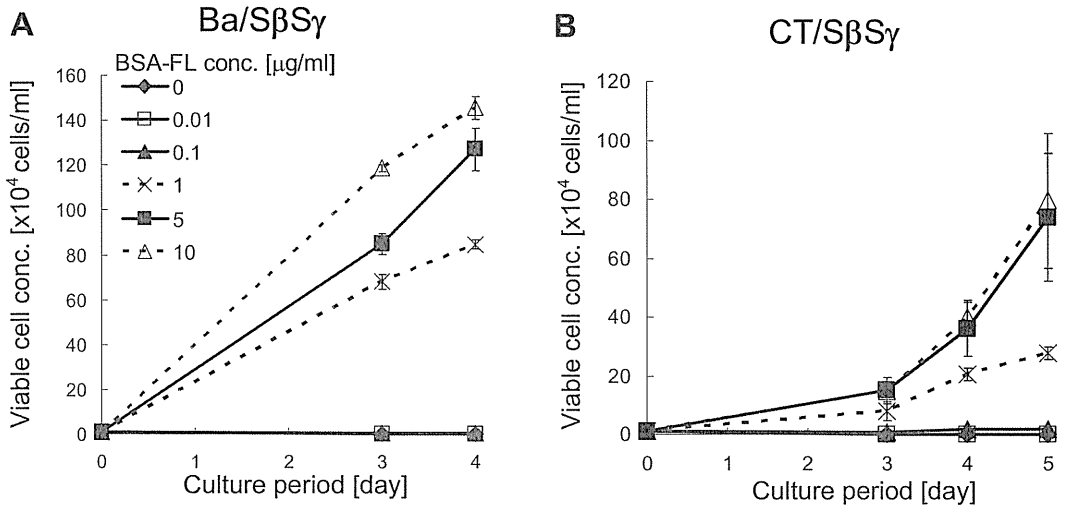

Fig. 4. BSA-FL-dependent cell growth of the transfectants/transductants. BSA-FL-selected Ba/SβSγ (A) and CT/SβSγ (B) were inoculated into 24-well plates at day 0 (10^4 cell well) and cultured with indicated concentrations of BSA-FL. Viable cell concentration in triplicates was plotted with average and 1 SD.

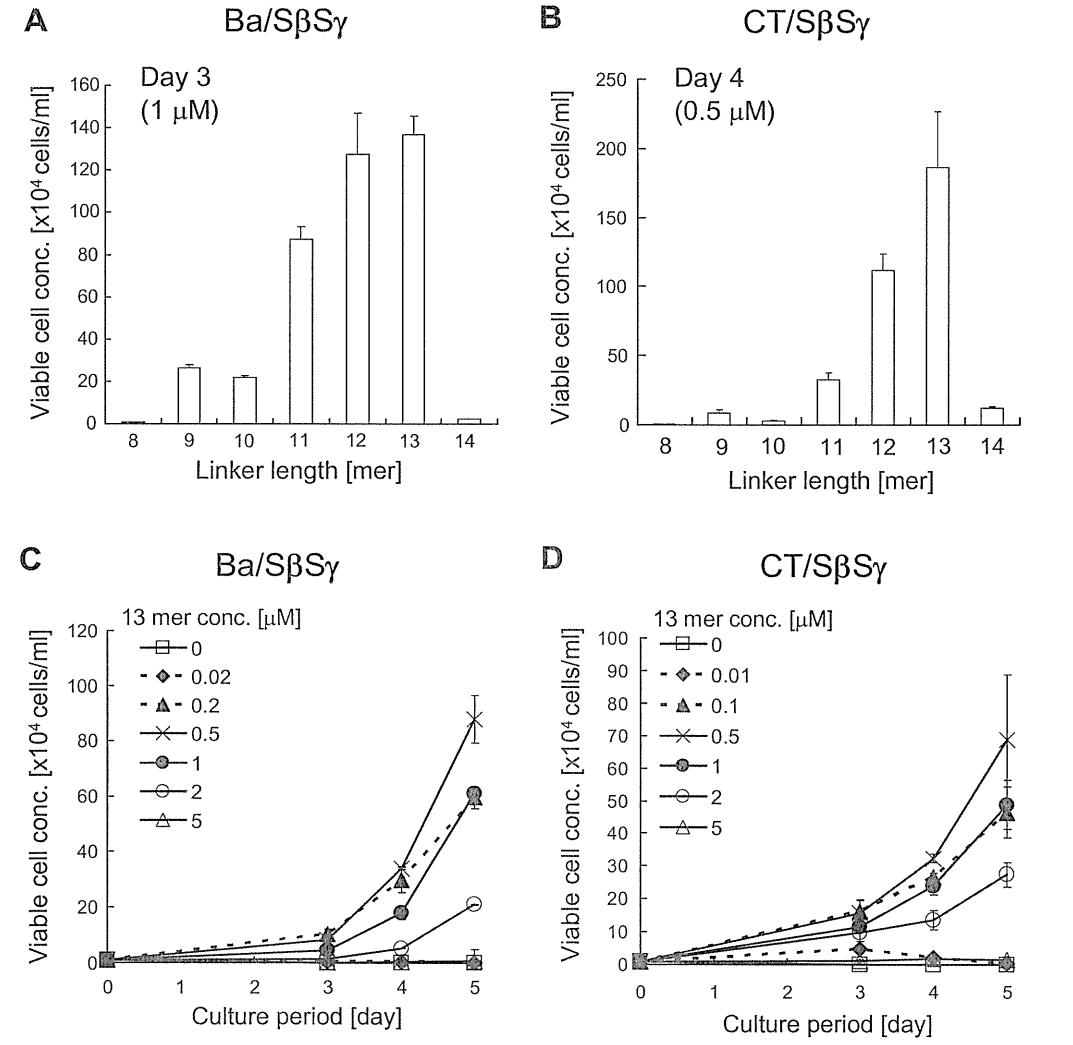

Fig. 5. FL-dimer-dependent cell growth of the transfectants/transductants. Ba/SβSγ (A) and CT/SβSγ (B) were inoculated into 24-well plates at 10^4 and 5×10^4 cells/we respectively, and cultured with various FL-dimers. Ba/SβSγ (C) and CT/SβSγ (D) were inoculated into 24-well plates at 10^4 cells/well and cultured with indicate concentrations of FL-dimer-13. Viable cell concentration in triplicates was plotted with average and 1 SD.

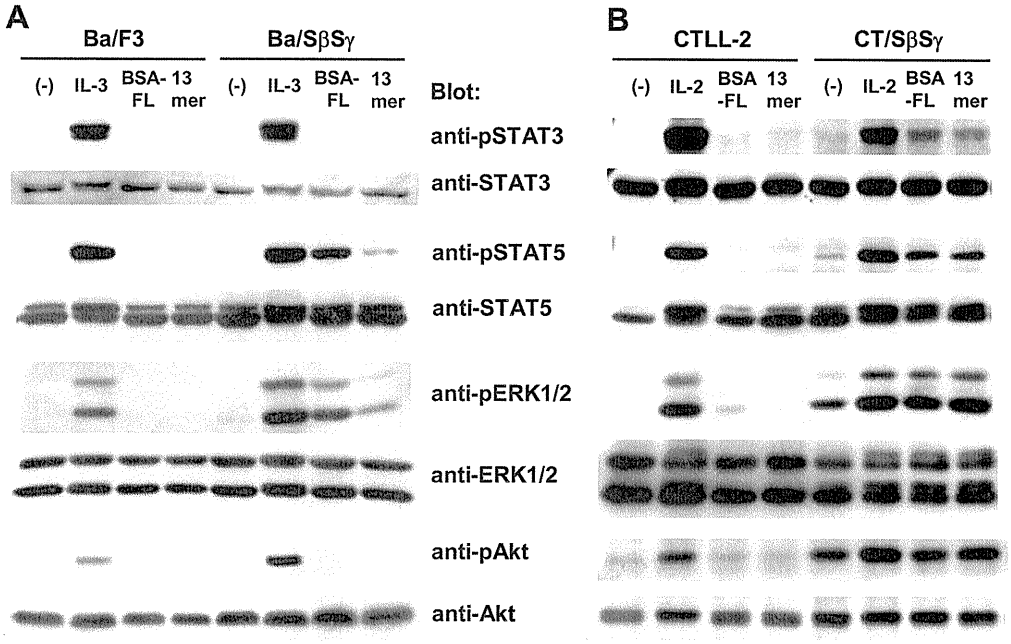

Fig. 6. Signal transduction to STAT3, STAT5, ERK1/2 and Akt. (A) Ba/F3 and Ba/SβSγ were stimulated with or without ligand (1 ng/ml IL-3, 5 μg/ml BSA-FL or 0.5 μM FL-dimer-13), and (B) CTLL-2 and CT/SβSγ were stimulated with or without ligand (2 ng/ml IL-2, 5 μg/ml BSA-FL or 0.5 μM FL-dimer-13). Western blot analysis was performed with anti-phospho STAT3, anti-phospho STAT5, anti-phospho-ERK1/2 and anti-phospho-Akt antibodies to detect phosphorylated form of each molecule, and with anti-STAT3, anti-STAT5, anti-ERK1/2 and anti-Akt antibodies to detect the whole molecules.

3.5. Chimeric IL-2R is functional in murine primary T cells

Murine primary T cells were transduced with chimeric IL-2Rs to confirm whether the chimeras are also functional in controlling a growth of primary T cells. To obtain high titers of retroviruses capable of transducing primary T cells with high efficiency, VSV-G pseudotyped retroviruses were prepared [40]. Retroviral packaging cell line, 293GPG was transduced with pGCDNsam-Sβ-IG or pGCDNsam-Sγ-IK (Fig. 7A), resulting in stable virus-producing cell lines named GPG/Sβ-IG or GPG/Sγ-IK. Sβ-IG encodes chimeric Sβ chain and EGFP genes, whereas Sγ-IK encodes chimeric Sγ chain and Kusabira Orange (KO) genes. The supernatants of GPG/Sβ-IG and GPG/Sγ-IK were 100-fold concentrated by centrifugation and used for co-transduction of murine primary T cells. The T cells expressing the chimeric Sβ chain and the chimeric Sγ chain are able to be distinguished by EGFP and KO fluorescence, respectively. Murine T cells were also co-transduced with mock vectors encoding IG and IK genes as a negative control.

Three days after transduction, EGFP and KO double positive (mock), Sβ-IG single positive (Sβ), Sγ-IK single positive (Sγ) and Sβ-IG and Sγ-IK double positive T cells (SβSγ) were sorted using fluorescence-activated cell sorter. The isolated T cells were cultured in the medium with no ligand, 5 μg/ml BSA-FL, or 10 ng/ml IL-2 for three days, followed by measuring viable cell numbers using flow cytometry (Fig. 7B). In SβSγ-transduced T cells, viable cell number was about 9-fold increased by addition of BSA-FL as compared to the cells cultured with no ligand. In Sβ-transduced T cells, viable cell number in the presence of BSA-FL was about 3-fold greater than that with no ligand. These data indicate that the SβSγ chimera is presumably functional in primary T cells, and that the Sβ chimera alone might transduce a subtle anti-apoptotic signal.

4. Discussion

In this study, we constructed an antibody/IL-2R chimera named SβSγ, which can recognize fluorescein and transduce a growth signal independent of IL-2. Several studies using transgenic mice constitutively expressing IL-2Rα and/or IL-2Rβ, or IL-4R/IL-2Rβ chimera demonstrated that $CD8^+$ T cells from these mice showed IL-2- or IL-4-responsive proliferation [27–29]. Thus, exogenous expression of IL-2R or IL-2R chimera on T cells would be capable of inducing T cells to grow through IL-2 signaling. In our previous studies, we established an antigen-mediated genetically modified cell amplification (AMEGA) system employing an antibody/receptor chimera that triggers a growth signal in response to a cognate antigen, HEL [14] or fluorescein [15]. Based on this AMEGA concept, ScFv/IL-2Rβ plus ScFv/IL-2Rγ (SβSγ) were constructed to selectively expand genetically modified T cells, since heterodimerization of the cytoplasmic domains of IL-2Rβ and γ chains are sufficient for IL-2R signal transduction [30]. When introduced into Ba/F3 and CTLL-2 cells, the SβSγ chimera induced selective expansion of genetically modified cells in the presence of BSA-FL. Furthermore, the proliferation of Ba/F3 and CTLL-2 that were transfected with SβSγ gene was successfully controlled simply by addition of BSA-FL or FL-dimer as a cognate ligand.

According to the results from the cell proliferation assay, both Ba/SβSγ and CT/SβSγ demonstrated strictly ligand dose-dependent cell growth. Therefore, the SβSγ chimera could be useful to regulate genetically modified T cell growth in vitro and in vivo. Concerning the in vivo application of the chimera, the target cells are favorable to be expanded by a dimeric fluorescein molecule that is expected to have low immunogenicity. We used a series of dimerized fluorescein (FL-dimers) tethered with a palindromic oligo-DNA linker. To our surprise, both Ba/SβSγ and CT/SβSγ could hardly grow in the presence of FL-dimer-8, -9, -10 and -14. Interestingly, FL-dimer-13 greatly promoted the cell growth while FL-dimer-14 did not, though the lengths of their linkers are almost equal when they are annealed. As the linker of FL-dimer-13 includes a thymine residue at its 5′ end that makes it incomplete palindrome, this linker may have more flexibility than that of FL-dimer-14. Thus, the differential flexibility between FL-dimer-13

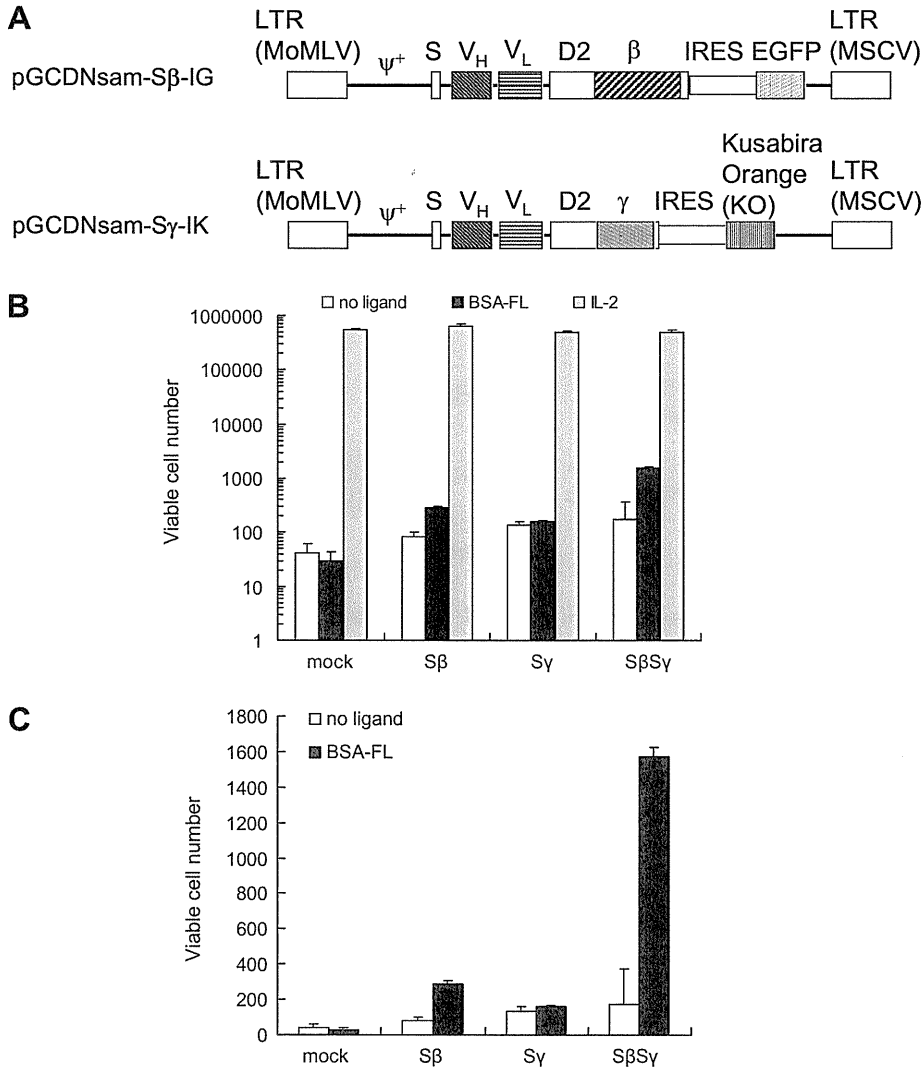

Fig. 7. Cell growth analysis of murine primary T cell-transductants. (A) The constructs of chimeric IL-2R vectors for transduction of murine primary T cells. pGCDNsam retroviral vector has 5′ MoMLV LTR, 3′ MSCV LTR and an extended packaging signal (Ψ^+). (B) The mouse primary T cells were inoculated into 48-well plates at 1.5×10^5 cells/well and cultured in the medium with no ligand, 5 μg/ml BSA-FL, or 10 ng/ml IL-2 for three days. Viable cell number per well in triplicates was plotted with average and 1 SD. (C) The cells cultured with no ligand and with BSA-FL are compared using the data in (B).

and -14 might contribute to the difference of their cell growth-promoting function, while the length of FL-dimer-8, -9 and -10 might be too short to activate the SβSγ chimera. The optimal FL-dimer for the signal transduction via the SβSγ chimera was FL-dimer-12 or -13 for Ba/SβSγ and FL-dimer-13 for CT/SβSγ. These FL-dimers were similar to the optimal FL-dimer to activate a ScFv-gp130 chimera [15]. However, the growth activity via the SβSγ chimera is highly dependent on the length of FL-dimer, around 40–45 Å, in contrast to that via the ScFv-gp130 chimera, which stimulated cell growth with all lengths of FL-dimers. The optimal concentration of FL-dimer-13 for the SβSγ chimera was around 0.5 μM, which is also similar to that for ScFv-gp130 chimera. The inhibitory effect of cell growth at higher concentration of FL-dimer might be due to the preferred formation of 1:1 FL-dimer–receptor complex suppressing receptor dimerization.

Although the cell growth assay showed that both Ba/SβSγ and CT/SβSγ proliferated with similar ligand dose-dependency, immunoblot analyses indicate that the phosphorylation states of the signal transducers were greatly different between these two cell lines. STAT5 and ERK were phosphorylated in both Ba/SβSγ and CT/SβSγ when they were stimulated by BSA-FL or by FL-dimer-13, whereas STAT3 and Akt were not phosphorylated in Ba/SβSγ stimulated by the same ligands. Despite the lack of activation of STAT3 and Akt, Ba/SβSγ was able to proliferate in the presence of the ligands. These data of Ba/SβSγ are consistent with the earlier report that used Ba/F3 cells expressing randomly mutated STAT5 [31]. The report showed that the cells expressing an active form of STAT5 could grow without IL-3. Because activation of STAT5 may be sufficient for a chimeric IL-2R-mediated cell proliferation of Ba/SβSγ, the cells which were incapable of activating STAT3 and Akt could be selected by BSA-FL stimulation unlike CTLL-2 transfectant. The major difference between CTLL-2 and Ba/F3 cells is that CTLL-2 cells express wild-type IL-2Rα, whereas Ba/F3 cells do not. It has been reported that the interaction of the cytoplasmic domain of IL-2Rβ with that of IL-2Rα leads to conformational changes of IL-2Rβ [32,33]. Therefore, the existence of IL-2Rα might be a determinant for the difference of the activation state of STAT3 and Akt between Ba/SβSγ and CT/SβSγ. Nevertheless, as the SβSγ chimera successfully mimics wild-type IL-2R signaling in response to BSA-FL or FL-dimer in CT/SβSγ, we demonstrated for the first time that genetically modified T cells could be selectively expanded by a small hapten molecule.

The chimera was also functional in murine primary T cells. The SβSγ-transduced T cells showed the increased cell viability by addition of BSA-FL, indicating that the chimera has an anti-apoptotic activity in response to BSA-FL. Although BSA-FL addition increased viable cell number in SβSγ-transduced T cells, apparent cell growth was not observed. It may be because culture period was too short for the cells to grow via signals from the chimera instead of IL-2 signaling, since even cultured cell lines, Ba/SβSγ and CT/SβSγ cells, also did not proliferate in first several days of selection. To confirm this hypothesis, it is required to prolong the culture period. Interestingly, Sβ-transduced T cells also showed slight increase of viable cell number by the addition of BSA-FL. As Sβ-transduced T cells do not express Sγ chains associated with Jak3, Sβ chains might form homodimers or homooligomers to transduce Jak3-independent anti-apoptotic signals in primary T cells [3].

These data suggest that the SβSγ chimera could be utilized for the expansion of genetically modified T cells. The genetic modification of T cells is a promising approach to improve anti-cancer therapeutic effect as well as to investigate T cell function. For adoptive transfer immunotherapy using genetically modified T cells, ex vivo and in vivo T cell expansion and selection procedures are required. The selection of genetically modified T cells using cytotoxic drugs, however, causes significant cell loss and often provokes survival of undesired cells in which the transgene is not stably integrated [34]. Our system could resolve this problem, because our chimeric IL-2Rs can select genetically modified T cells by promoting their cell growth, and non-transduced cells would not survive in long-term culture without IL-2. Considering about in vivo expansion of T cells, administration of high-dose IL-2 has been the only way to expand T cells in clinical trials. However, high-dose IL-2 not only causes undesirable side effects like an inflammation, but also activates regulatory T cells that function as negative regulators of immune responses, leading to apoptosis of the effector T cells [35–37]. In this study, we succeeded in controlling cell growth in vitro using a fluorescein-specific ScFv-based chimeric IL-2R. Unlike IL-2, our system has a potential for in vivo selection without toxicity, because the SβSγ chimera enables only gene-modified T cells to proliferate in response to fluorescein derivatives, which are based on a small hapten, fluorescein, having no immunogenicity. Moreover, as there are a countless number of antigen–antibody pairs, ScFv-based chimera has the advantage that various antigens could be used for regulating cell growth as a cognate ligand. The system also has a potential for the regulation of natural immune system. It is known that NK cells, which can attack non-MHC-expressing tumor cells, are also activated by IL-2 [38,39]. Therefore, our chimeric IL-2R may be useful to control proliferation of both T cells and NK cells for an effective anti-tumor immunotherapy.

Acknowledgments

We are grateful to Dr. K. Todokoro (RIKEN) for pME-IL-2Rβ, Dr. T. Kitamura (University of Tokyo) for the retroviral expression system and Dr. I.M. Tomlinson (Domantis, Cambridge, UK) for anti-FL antibody ScFv. This work was supported by Grants-in-Aid for Scientific Research (A) 18206083 (TN) from the MEXT, Japan and the Global COE Program for Chemistry Innovation.

References

[1] Stauber DJ, Debler EW, Horton PA, Smith KA, Wilson IA. Crystal structure of the IL-2 signaling complex: paradigm for a heterotrimeric cytokine receptor. Proc Natl Acad Sci USA 2006;103:2788–93.
[2] Wang X, Rickert M, Garcia KC. Structure of the quaternary complex of interleukin-2 with its α, β, and γ_c receptors. Science 2005;310:1159–63.
[3] Nelson BH, Lord JD, Greenberg PD. Cytoplasmic domains of the interleukin-2 receptor beta and gamma chains mediate the signal for T-cell proliferation. Nature 1994;369:333–6.
[4] Leen AM, Rooney CM, Foster AE. Improving T cell therapy for cancer. Annu Rev Immunol 2007;25:243–65.
[5] Knutson KL, Almand B, Mankoff DA, Schiffman K, Disis ML. Adoptive T-cell therapy for the treatment of solid tumours. Exp Opin Biol Ther 2002;2:1–12.
[6] Rosenberg SA. Progress in human tumour immunology and immunotherapy. Nature 2001;411:380–4.
[7] Tey SK, Bollard CM, Heslop HE. Adoptive T-cell transfer in cancer immunotherapy. Immunol Cell Biol 2006;84:281–9.
[8] Cheever MA, Chen W. Therapy with cultured T cells: principles revisited. Immunol Rev 1997;157:177–94.
[9] Dudley ME, Rosenberg SA. Adoptive-cell-transfer therapy for the treatment of patients with cancer. Nat Rev Cancer 2003;3:666–75.
[10] Dudley ME, Wunderlich JR, Yang JC, Sherry RM, Topalian SL, Restifo NP, et al. Adoptive cell transfer therapy following non-myeloablative but lymphodepleting chemotherapy for the treatment of patients with refractory metastatic melanoma. J Clin Oncol 2005;23:2346–57.
[11] Koike N, Pilon-Thomas S, Mule JJ. Nonmyeloablative chemotherapy followed by T-cell adoptive transfer and dendritic cell-based vaccination results in rejection of established melanoma. J Immunother 2008;31:402–12.
[12] Kragel AH, Travis WD, Feinberg L, Pittaluga S, Striker LM, Roberts WC, et al. Pathologic findings associated with interleukin-2-based immunotherapy for cancer: a postmortem study of 19 patients. Hum Pathol 1990;21:493–502.
[13] Rosenberg SA, Lotze MT, Muul LM, Leitman S, Chang AE, Ettinghausen SE, et al. Observations on the systemic administration of autologous lymphokine-activated killer cells and recombinant interleukin-2 to patients with metastatic cancer. N Engl J Med 1985;313:1485–92.
[14] Kawahara M, Ueda H, Morita S, Tsumoto K, Kumagai I, Nagamune T. Bypassing antibiotic selection: positive screening of genetically modified cells with an antigen-dependent proliferation switch. Nucleic Acids Res 2003;31:e32.
[15] Kawahara M, Kimura H, Ueda H, Nagamune T. Selection of genetically modified cell population using hapten-specific antibody/receptor chimera. Biochem Biophys Res Commun 2004;315:132–8.
[16] Ueda H, Kawahara M, Aburatani T, Tsumoto K, Todokoro K, Suzuki E, et al. Cell-growth control by monomeric antigen: the cell surface expression of lysozyme-specific Ig V-domains fused to truncated Epo receptor. J Immunol Methods 2000;241:159–70.
[17] Sogo T, Kawahara M, Tsumoto K, Kumagai I, Ueda H, Nagamune T. Selective expansion of genetically modified T cells using an antibody/interleukin-2 receptor chimera. J Immunol Methods 2008;337:16–23.
[18] Kawahara M, Ogo Y, Ueda H, Nagamune T. Improved growth response of antibody/receptor chimera attained by the engineering of transmembrane domain. Protein Eng Des Sel 2004;17:715–9.
[19] Kaneko E, Kawahara M, Tsumoto K, Kumagai I, Ueda H, Nagamune T. Antigen-mediated genetically modified cell amplification (AMEGA) with single vector transduction. J Chem Eng Japan 2004;37:1259–64.
[20] Palacios R, Steinmetz M. IL3-dependent mouse clones that express B-220 surface antigen, contain Ig genes in germ-line configuration, and generate B lymphocyte in vivo. Cell 1985;41:727–34.
[21] Gillis S, Smith KA. Long term culture of tumour-specific cytotoxic T cells. Nature 1977;268:154–6.
[22] Brielmeier M, Bechet J, Falk MH, Pawlita M, Polack A, Bornkamm GW. Improving stable transfection efficiency: antioxidants dramatically improve the outgrowth of clones under dominant marker selection. Nucleic Acids Res 1998;26:2082–5.
[23] Morita S, Kojima T, Kitamura T. Plat-E: an efficient and stable system for transient packaging of retroviruses. Gene Ther 2000;7:1063–6.
[24] Ellery JM, Nicholls PJ. Alternate signaling pathways from the interleukin-2 receptor. Cytokine Growth Factor Rev 2002;13:27–40.
[25] Asao H. Mechanism of interleukin 2-induced signal transduction. Yamagata Med J 2003;21:141–54.
[26] Jiang K, Zhong B, Ritchey C, Gilvary DL, Hong-Geller E, Wei S, et al. Regulation of Akt-dependent cell survival by Syk and Rac. Blood 2003;101:236–44.
[27] Asano M, Ishida Y, Sabe H, Kondo M, Sugamura K, Honjo T. IL-2 can support growth of $CD8^+$ T cells but not $CD4^+$ T cells of human IL-2 receptor beta-chain transgenic mice. J Immunol 1994;153:5373–81.
[28] Gasser S, Corthesy P, Beerman F, MacDonald HR, Nabholz M. Constitutive expression of a chimeric receptor that delivers IL-2/IL-15 signals allows antigen-independent proliferation of $CD8^+$ $CD44^{high}$ but not other T cells. J Immunol 2000;164:5659–67.
[29] Nishi M, Ishida Y, Honjo T. Expression of functional interleukin-2 receptors in human light chain/Tac ransgenic mice. Nature 1988;331:267–9.
[30] Nakamura Y, Russell SM, Mess SA, Friedmann M, Erdos M, Francois C, et al. Heterodimerization of the IL-2 receptor beta- and gamma-chain cytoplasmic domains is required for signalling. Nature 1994;369:330–3.
[31] Onishi M, Nosaka T, Misawa K, Mui AL-F, Gorman D, McMahon M, et al. Identification and characterization of a constitutively active STAT5 mutant that promotes cell proliferation. Mol Cell Biol 1998;18:3871–9.
[32] Goldsmith MA, Amaral MC, Greene WC. Ligand binding by the IL-2 receptor is modulated by intracellular determinants of the IL-2 receptor β-chain. J Immunol 1995;154:2033–40.
[33] Ellery JM, Nicholls P. Possible mechanism for the alpha subunit of the interleukin-2 receptor (CD25) to influence interleukin-2 receptor signal transduction. Immunol Cell Biol 2002;80:351–7.
[34] Cooper LJN, Ausubel L, Gutierrez M, Stephan S, Shakeley R, Olivares S, et al. Manufacturing of gene-modified cytotoxic T lymphocytes for autologous cellular therapy for lymphoma. Cytotherapy 2006;8:105–17.

[35] Ahmadzadeh M, Rosenberg SA. IL-2 administration increases CD4$^+$ CD25^{hi} Foxp3$^+$ regulatory T cells in cancer patients. Blood 2006;107:2409–14.
[36] Pandiyan P, Zheng L, Ishihara S, Reed J, Lenardo MJ. CD4$^+$ CD25$^+$ Foxp3$^+$ regulatory T cells induce cytokine deprivation mediated apoptosis of effector CD4$^+$ T cells. Nat Immunol 2007;8:1353–62.
[37] Wei S, Kryczek I, Edwards RP, Zou L, Szeliga W, Banerjee M, et al. Interleukin-2 administration alters the CD4$^+$ FOXP3$^+$ T-cell pool and tumor trafficking in patients with ovarian carcinoma. Cancer Res 2007;67:7487–94.
[38] Mule JJ, Shu S, Schwarz SL, Rosenberg SA. Adoptive immunotherapy of established pulmonary metastases with LAK cells and recombinant interleukin-2. Science 1984;225:1487–9.
[39] Bradley M, Zeytun A, Rafi-Janajreh A, Nagarkatti PS, Nagarkatti M. Role of spontaneous and interleukin-2-induced natural killer cell activity in the cytotoxicity and rejection of Fas$^+$ and Fas$^-$ tumor cells. Blood 1998;92:4248–55.
[40] Suzuki A, Obi K, Urabe T, Hayakawa H, Yamada M, Kaneko S, Onodera M, Mizuno Y, Mochizuki H. Feasibility of ex vivo gene therapy for neurological disorders using the new retroviral vector GCDNsap packaged in the vesicular stomatitis virus G protein. J Neurochem 2002;82:953–60.
[41] Kaneko S, Nagasawa T, Nakauchi H, Onodera M. An in vivo assay for retrovirally transduced human peripheral T lymphocytes using nonobese diabetic/severe combined immunodeficiency mice. Exp Hematol 2005;33:35–41.
[42] Sanuki S, Hamanaka S, Kaneko S, Otsu M, Karasawa S, Miyawaki A, Nakauchi H, Nagasawa T, Onodera M. A new red fluorescent protein that allows efficient marking of murine hematopoietic stem cells. J Gene Med 2008;10:965–71.

Int J Hematol (2009) 89:24–33
DOI 10.1007/s12185-008-0212-2

ORIGINAL ARTICLE

Transcriptional profiling of hematopoietic stem cells by high-throughput sequencing

Yoshimi Yashiro · Hideo Bannai · Takashi Minowa · Tomohide Yabiku · Satoru Miyano · Mitsujiro Osawa · Atsushi Iwama · Hiromitsu Nakauchi

Received: 19 August 2008 / Revised: 1 October 2008 / Accepted: 23 October 2008 / Published online: 3 December 2008

Abstract Microarray analysis has made it feasible to carry out extensive gene expression profiling in a single assay. Various hematopoietic stem cell (HSC) populations have been subjected to microarray analyses and their profiles of gene expression have been reported. However, this approach is not suitable to identify novel transcripts or for profiling of genes with low expression levels. To obtain a detailed gene expression profile of $CD34^-$c-$Kit^+Sca\text{-}1^+$lineage marker-negative (Lin^-) ($CD34^-$KSL) HSCs, we constructed a $CD34^-$KSL cDNA library, performed high-throughput sequencing, and compared the generated profile with that of another HSC fraction, side population (SP) Lin^- (SP Lin^-) cells. Sequencing of the 5′-termini of about 9,500 cDNAs from each HSC library identified 1,424 and 2,078 different genes from the $CD34^-$KSL and SP Lin^- libraries, respectively. To exclude ubiquitously expressed genes including housekeeping genes, digital subtraction was successfully performed against EST databases of other organs, leaving 25 HSC-specific genes including five novel genes. Among 4,450 transcripts from the $CD34^-$KSL cDNA library that showed no homology to the presumable protein-coding genes, 29 were identified as strong candidates for

Electronic supplementary material The online version of this article (doi:10.1007/s12185-008-0212-2) contains supplementary material, which is available to authorized users.

Y. Yashiro · M. Osawa · A. Iwama · H. Nakauchi
Division of Stem Cell Therapy,
Center for Stem Cell and Regenerative Medicine,
The Institute of Medical Science, University of Tokyo,
Tokyo 108-8639, Japan

H. Bannai · T. Yabiku · S. Miyano
Laboratory of DNA Information Analysis,
Human Genome Center, The Institute of Medical Science,
University of Tokyo, Tokyo 108-8639, Japan

Present Address:
A. Iwama
Department of Cellular and Molecular Medicine,
Graduate School of Medicine, Chiba University,
Chiba 260-8670, Japan

H. Bannai
Department of Informatics, Kyushu University,
744 Moto-oka, Nishi-ku, Fukuoka 819-0395, Japan

Present Address:
T. Yabiku
Interdisciplinary Intelligent Systems Engineering Course,
Graduate School of Engineering and Science,
Ryukyu University, Okinawa 903-0213, Japan

T. Minowa
Hitachi, Ltd, Life Science Group,
Saitama 350-1165, Japan

Present Address:
T. Minowa
Nanotechnology Innovation Center,
National Institute for Materials Science,
Ibaraki 305-0047, Japan

Present Address:
M. Osawa
Department of Developmental Biology,
University of Texas Southwestern Medical Center,
5323 Harry Hines Boulevard, Dallas, TX 75390-9133, USA

H. Nakauchi (✉)
Laboratory of Stem Cell Therapy,
Center for Experimental Medicine,
The Institute of Medical Science,
University of Tokyo, Tokyo 108-8639, Japan
e-mail: nakauchi@ims.u-tokyo.ac.jp

mRNA-like non-coding RNAs by in silico analyses. Our cyclopedic approaches may contribute to understanding of novel molecular aspects of HSC function.

Keywords Hematopoietic stem cells · High-throughput sequencing · Non-coding RNA

1 Introduction

Hematopoietic stem cells (HSCs) have the capacity to self-renew as well as the ability to differentiate into all adult hematopoietic lineages and to maintain hematopoiesis throughout the lifetime of the animal. With recent advances in cell separation systems, we now have access to highly purified HSCs. We have previously reported that in adult mouse bone marrow (BM), $CD34^{low/-}$c-$Kit^{+}Sca\text{-}1^{+}$lineage markers-negative (Lin^{-}) ($CD34^{-}$KSL) cells represent HSCs with long-term marrow repopulating ability [1]. 'Side population' (SP) cell sorting also was applied to identify HSCs [2]. SP cells are detected by their ability to efflux Hoechst 33342 dye through an adenosine triphosphate-binding cassette membrane transporter [3]. Both fractions, $CD34^{-}$KSL and SP Lin^{-}, in mouse BM are highly enriched for long-term BM repopulating cells. The very low numbers of such repopulating cells, however, have hampered studies of HSCs, leaving the molecular nature of HSCs unknown. Recent technological innovation is overcoming this disadvantage. Microarray analyses in particular have made it feasible to carry out extensive gene expression profiling in a single assay. However, this approach is not suitable to identify novel transcripts or for profiling of genes with low expression levels. Various hematopoietic stem/progenitor cell fractions have been characterized by microarray analyses and cDNA subtraction, including mouse SP c-$Kit^{+}Sca\text{-}1^{hi}Lin^{-}$, $Thy1.1^{lo}$ c-$Kit^{+}Sca\text{-}1^{hi}Lin^{-}$, c-$Kit^{+}Sca\text{-}1^{hi}Lin^{-}Rho^{lo}$, and fetal liver c-$Kit^{+}Sca\text{-}1^{hi}Lin^{-}AA4.1^{+}$ [4–13]. Lists of HSC-specific genes are now available from several online databases such as Stem Cell Database (SCDb; http://stemcell.princeton.edu/) [12]. However, the gene expression profiles of $CD34^{-}$KSL cells have never been directly compared with those of other HSC populations.

In this study, we constructed cDNA libraries from $CD34^{-}$KSL and SP Lin^{-} cells by using long-distance PCR amplification of full-length cDNA, and performed high-throughput sequencing of the cDNAs yielded. Using digital subtraction against ESTs from other organ databases, we detected 25 novel genes. Furthermore, we identified 29 candidates for mRNA-like non-coding RNAs by in silico analysis. Our cyclopedic approach provides information valuable in understanding molecular aspects of HSC regulation.

2 Materials and methods

2.1 Mice

C57BL/6 (B6-Cre) mice were purchased from SLC Japan, Inc. (Hamamatsu, Japan).

2.2 Isolation of HSCs

Mouse $CD34^{-}$KSL and SP Lin^{-} cells were purified from BM cells of 2-month-old mice. Low-density cells were isolated on Lymphoprep (1.086 g/ml; Nycomed, Oslo, Norway), and were stained with an antibody cocktail consisting of biotinylated anti-Gr-1, -Mac-1, -B220, -CD4, -CD8, and -Ter-119 mAbs (PharMingen, San Diego, CA, USA). Lineage-positive cells were depleted by passage over a MACS separation column with goat anti-rat IgG microbeads (Miltenyi Biotec, Bergisch Gladbach, Germany). The cells were further stained with fluorescein isothiocyanate (FITC)-conjugated anti-CD34, phycoerythrin (PE)-conjugated anti-Sca-1, and allophycocyanin (APC)-conjugated anti-c-Kit antibodies (PharMingen). Biotinylated antibodies were detected with streptavidin-APC-Cy7 (Molecular Probes, Eugene, OR, USA). SP Lin^{-} cells were stained with Hoechst 33342 after depleting lineage-positive cells. HSCs were isolated by fluorescence-activated cell sorting (FACS) using a MoFlo flow cytometer (DAKO Cytomation, Fort Collins, CO, USA).

2.3 Construction of HSC cDNA libraries

Total RNA was isolated from 6,000 $CD34^{-}$KSL and 10,000 SP Lin^{-} cells using ISOGEN-LS solution (Nippon Gene, Tokyo, Japan). Total RNA was subjected to full-length cDNA synthesis using a SMART™ PCR cDNA synthesis kit (Clontech, Palo Alto, CA, USA), which is based on SMART cDNA technology and cDNA amplification by long-distance PCR. $CD34^{-}$KSL cDNA was subcloned into the λTripEx2 phage vector (Clontech). SP Lin^{-} cDNA was subcloned into the pMX retrovirus vector [14].

2.4 Sequencing

XL1-Blue *Escherichia coli* cells were infected with the $CD34^{-}$KSL phage library and were subcloned by plating on L Broth (LB) plates. cDNA inserts were initially amplified by standard PCR procedures on a PE 9600 thermal cycler (Applied Biosystems, Foster City, CA, USA) using the following primers: sense, 5′-CTCCGAGATCTGGACG AGC-3′, and antisense, 5′-CGTT GTAAAACGACGGC CAGTG-3′. PCR products were purified using ExoSAP-IT (Amersham Biosciences, Uppsala, Sweden) and were

sequenced using the following primer: 5′-TCTCGG GAAGCGCGCCAT-3′. The SP Lin$^-$ library was transfected by electroporation into JM109 *E. coli* cells, which then were plated on LB plates. Plasmid DNA was prepared by the alkaline-SDS method and purified by multiscreen FB filtration (Millipore, Billerica, MA, USA). Products were sequenced using the following primer: 5′-GACCTTA CACAGTCCTGCTGAC-3′.

2.5 Analysis of sequence data

A homology search of HSC library clones was performed against the RefSeq nucleotide sequence databases from the NCBI website (http://www.ncbi.nlm.nih.gov/BLAST/) using the BLASTN algorithm. Each HSC clone was assigned a Refseq identification number (ID) [15]. The clones showing the highest-scoring hits for both Identity (>95%) and Bitscore (>300.0) were selected for further analyses. Additional databases used for analyses included the Gene Ontology (GO) database from the Gene Ontology Consortium website (http://geneontology.org/) [16].

2.6 In silico subtraction

The EST databases for multiple organs, including small intestine (dbEST ID: 2601, 7229), heart (509, 5430), kidney (7215, 1300), liver (9742, 1299), and muscle (8902) were downloaded from the mouse UniGene website (http://www.ncbi.nlm.nih.gov/UniGene/). All genes were assigned a Refseq ID by BLASTN searching. Multi-organ ESTs were digitally subtracted from the HSC library clones. SCDb clones also were downloaded, assigned Refseq IDs, and compared with the HSC library clones.

2.7 Identification of putative non-coding RNAs

After homology with known protein-coding sequences according to BLASTN had been sought, remaining sequences were aligned to genomic sequence by using BLAT (http://www.genomeblat.com/genomeblat/index.asp). If they were aligned at >90% identify over >90% of their length, their cDNAs were kept; otherwise they were discarded. All of the homology searches against publicly available EST sequences were performed by BLASTN. Only EST sequences with an $E < 1.0e\text{-}100$ were regarded as corresponding to homologous mouse ESTs (ftp://ftp.ncbi.nih.gov/blast/db/est_mouse.Z). Sequences with *E*-values lower than 1.0e-50 were regarded as likely human and rat orthologous ESTs. Reverse hits were not considered.

2.8 Semi-quantitative RT-PCR

Semi-quantitative RT-PCR was carried out with normalized cDNA by quantitative PCR using TaqMan rodent GAPDH control reagent (Applied Biosystems) as described [17]. PCR products were separated on agarose gels and visualized by ethidium bromide staining.

3 Results

3.1 Cell sorting and library construction

Total RNA from 6,000 CD34$^-$KSL and 10,000 SP Lin$^-$ cells was subjected to full-length cDNA synthesis coupled with cDNA amplification by long-distance PCR. CD34$^-$KSL and SP Lin$^-$ cDNAs were, respectively, subcloned into the λTripEx2 phage vector and the pMX retrovirus vector. The sizes of the library were, respectively, 1.15×10^6 and 1.16 kb (Fig. 1). Although the two libraries were in different vectors, we used the same method for cDNA amplification and the average insert sizes were comparable with each other (CD34$^-$KSL 1.07 kb and SP Lin$^-$ 1.16 kb). Thus, we reasoned that the difference in the library construction methods did not cause any significant biases in gene expression profiles between the two populations.

3.2 Gene expression analysis

We sequenced the 5′-termini of about 9,500 cDNAs from each HSC library and compared them, using the BLASTN search algorithm, to a non-redundant database made available from the National Center for Biotechnology Information (NCBI). About 5,000 cDNAs from each library were determined to be identical to known genes in the NCBI database. These were sorted into non-overlapping sets of 1,424 and 2,077 different genes for CD34$^-$KSL and SP Lin$^-$, respectively (Fig. 2a). Most of the genes in our original collection (CD34$^-$KSL 775, SP Lin$^-$ 1,385) were represented by a single clone. In contrast, most of the genes represented by multiple cDNAs were housekeeping genes, including ubiquitin B (CD34$^-$KSL 43, SP Lin$^-$ 46), β-actin (CD34$^-$KSL 33, SP Lin$^-$ 36), ribosomal protein, and so on (Fig. 2b).

After assigning gene identities, we used reported GO to assign predictable functions to 1,034 of the CD34$^-$KSL cDNAs and 1,510 of the SP Lin$^-$ cDNAs in our set. We categorized genes by their products' subcellular localizations, biological processes, and molecular functions (Fig. 3).

We then compared gene profiles between the two HSC libraries and also with SCDb-listed HSC-specific genes

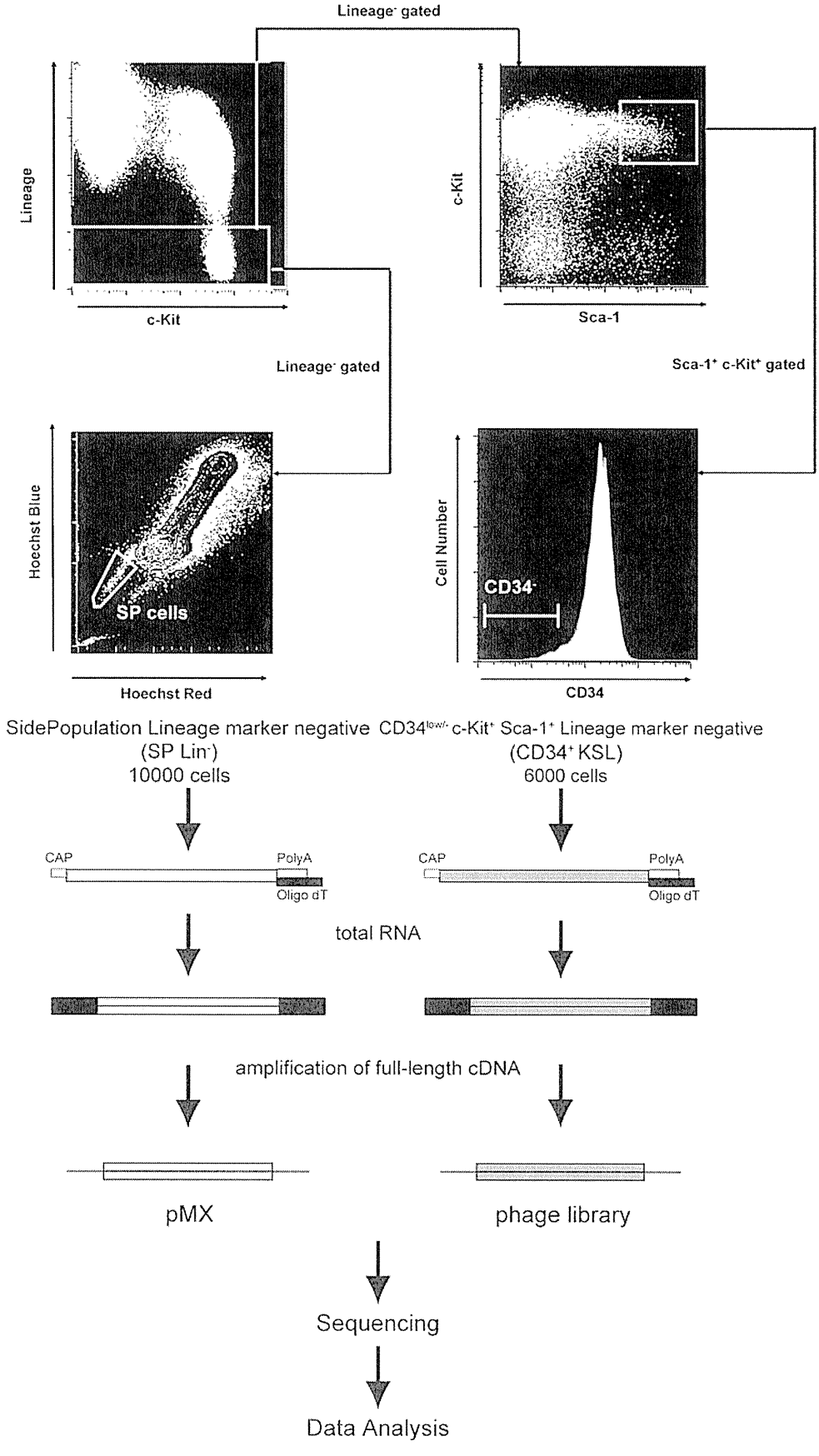

Fig. 1 Construction of the HSC cDNA libraries. Cell sorting gates for the two HSC fractions are depicted. Total RNA isolated from 6,000 $CD34^{-}KSL$ and 10,000 SP Lin^{-} cells was subjected to full-length cDNA s*ynthesis* and to cDNA amplification by long-distance PCR. $CD34^{-}KSL$ and SP Lin^{-} cDNAs were subcloned, respectively, into the λTripEx2 phage vector and the pMX retrovirus vector

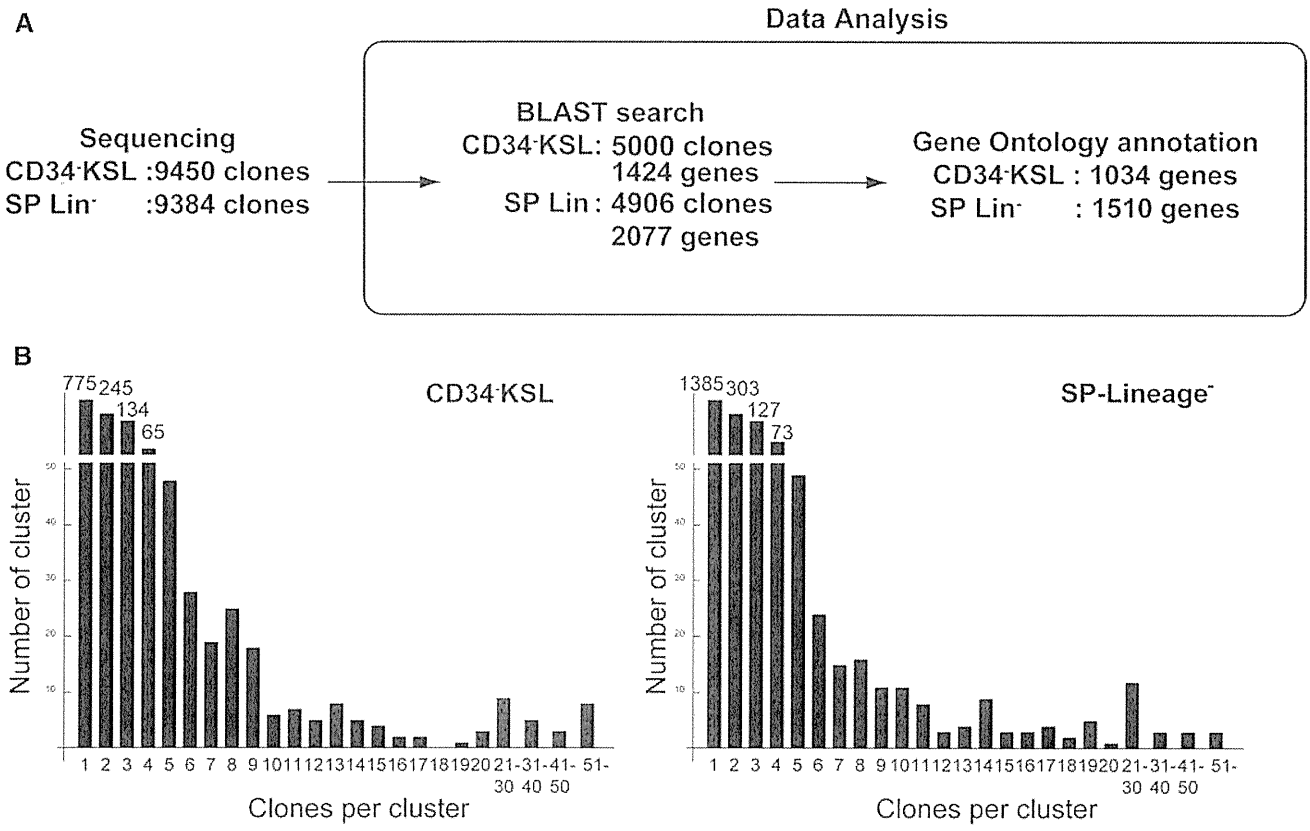

Fig. 2 Profiling of gene expression of hematopoietic stem cells by high-throughput sequencing. **a** Summary of the HSC clones identified by high-throughput sequencing. **b** Non-overlapping ESTs from CD34$^-$KSL and SP Lin$^-$ cells were assembled into clusters of singletons and contigs. The number of clusters (*Y*-axis) is plotted versus the number of clones in each cluster (*X*-axis)

[12] by using UniGene numbers to determine overlaps (Fig. 4a). To exclude ubiquitously expressed genes including housekeeping genes, digital subtraction was performed against ESTs from heart, muscle, liver, kidney, and intestine EST databases. After subtraction, 31 genes were determined to be in common between the two HSC libraries. Six of them were also included in the SCDb database (Fig. 4b). A detailed list of these genes is presented in Tables 1 and 2. Among 31 genes shared between the two HSC libraries, 25 genes appeared HSC-specific, a feature not previously reported. Of note was that five of them were novel (Fig. 4b). We next used RT-PCR to analyze these genes' expression profiles in CD34$^-$KSL and SP Lin$^-$ HSC populations. As shown in Fig. 5, we confirmed that several genes are specific to CD34$^-$KSL or to SP Lin$^-$. Others were expressed in both populations, although some genes that were not included in the SCDb database showed no HSC specificity (Table 3).

3.3 Identification of mRNA-like putative non-coding RNAs

Four thousand and four hundred and fifty clones from the CD34$^-$KSL cDNA library did not show any homology to the known protein-encoding genes in the NCBI database. We therefore computationally screened them to see if their products might include putative non-coding RNAs, the biological significance of which has recently been recognized [18, 19] (Fig. 6a).

Of these, 211 bore candidate sequences that matched the three-step criteria described in Methods (above). Among these 211, 112 clones (82 independent sequences) showed homology with known UniGene mouse ESTs. Of these 82, 55 sequences were hypothesized to represent protein-coding RNA, leaving 43 clones (29 independent sequences) as candidates for non-coding RNAs (Fig. 6b).

4 Discussion

With advances in technologies for HSC purification, many HSC populations have been subjected to gene expression profiling analyses. SCDb, one of the representative HSC databases, lists HSC-specific genes screened by high-throughput sequencing and microarray analysis of fetal liver AA4.1$^+$KSL cells and by microarray analysis of BM Rhodamine-123^{low}KSL cells. A list of HSC-specific genes has also been provided by detailed microarray analyses of

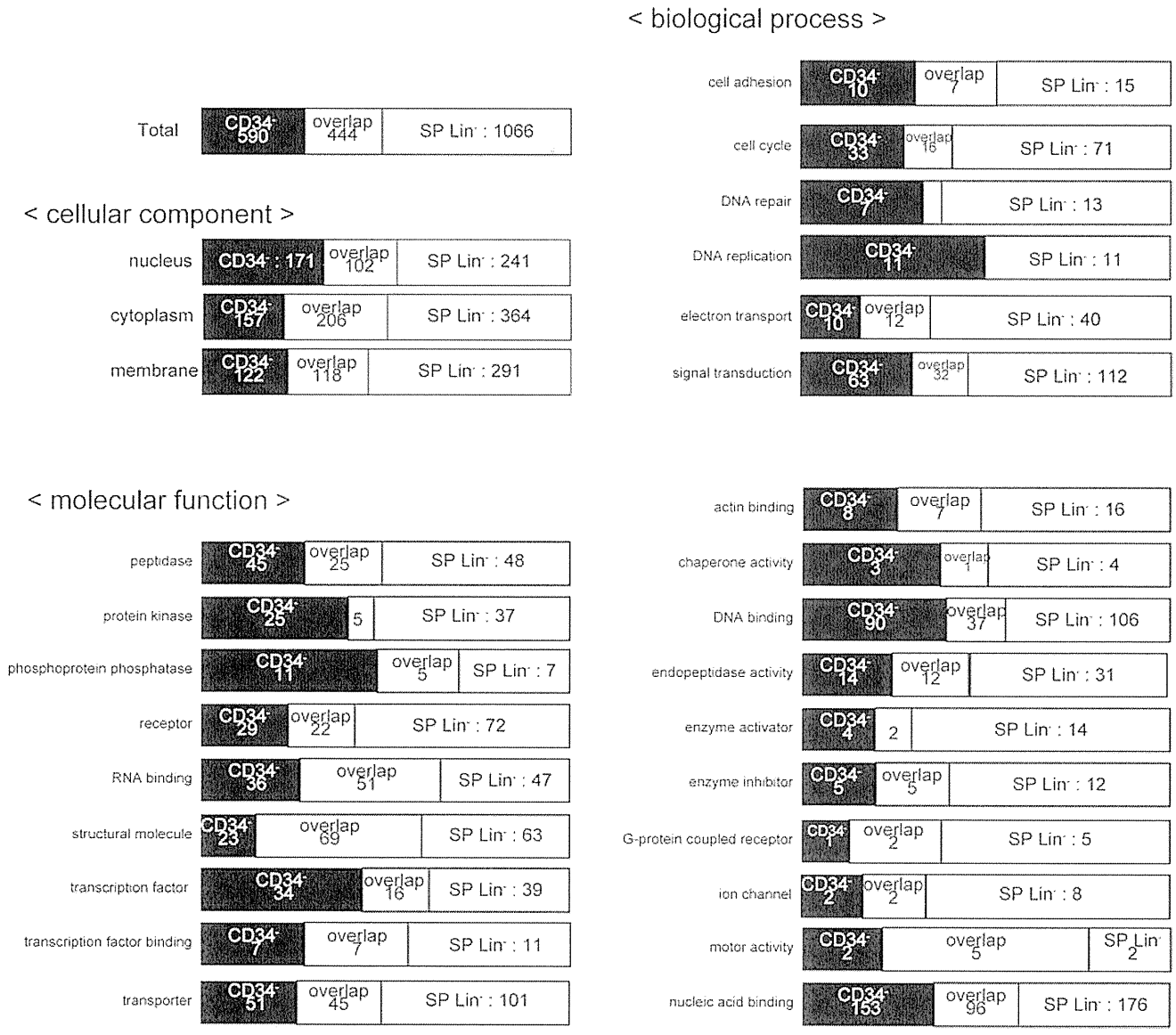

Fig. 3 Distribution of known or putative locus and functions of gene products for CD34$^-$KSL and SP Lin$^-$ genes determined by gene ontology. **a** Total, **b** cellular component, **c** molecular function, and **d** biological process

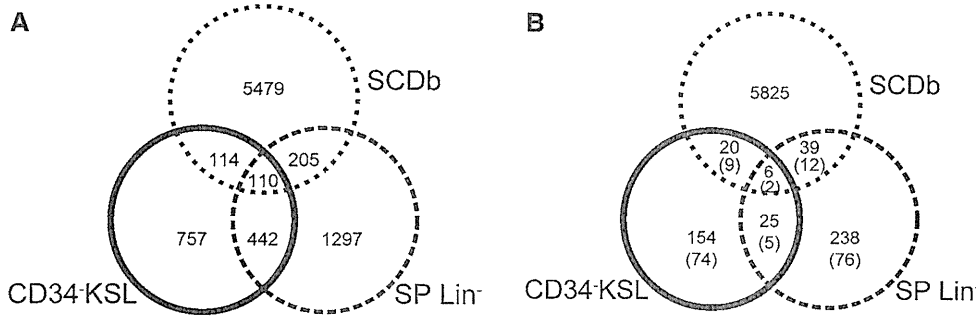

Fig. 4 Overlapping gene expression in HSCs. **a** Venn diagram detailing shared and distinct genes listed in SCDb or expressed by CD34$^-$KSL cells or by SP Lin$^-$ cells. **b** Venn diagram detailing shared and distinct genes expressed among CD34$^-$KSL cells, SP Lin$^-$ cells, and SCDb after in silico subtraction. The genes in EST databases for brain, heart, muscle, liver, kidney, and intestine were subtracted in silico from the HSC cDNAs

Table 1 Lists of genes identified as expressed in common among SCDb, CD34$^-$KSL, and SP Lin$^-$ libraries

Accession no.	Gene
NM 008114	Growth factor independent 1B
NM 028460	RIKEN cDNA 3110045G13 gene (3110045G13Rik)
NM 008595	Manic fringe homolog (Drosophila) (Mfng)
NM 022881	Regulator of G-protein signaling 18 (Rgs18)
NM 144886	Exosome component 2 (Exosc2)
XM 354694	Serine (or cysteine) proteinase inhibitor, clade A, member 3G (Serpina3g)

Table 2 Lists of genes identified as shared only between CD34$^-$KSL and SP Lin$^-$ libraries

Accession no.	Gene
NM 008187	Gene trap locus 3 (Gtl3)
NM 026042	RIKEN cDNA 2810405O22 gene (2810405O22Rik)
NM 026753	RIKEN cDNA 1110019N10 gene (1110019N10Rik)
XM 127929	RIKEN cDNA 4933421G18 gene (4933421G18Rik)
NM 144541	Brain and reproductive organ-expressed protein (Bre)
NM 145711	Thymocyte selection-associated HMG box gene (Tox)
NM 172148	cDNA sequence BC028440 (BC028440)
NM 009342	t-Complex testis expressed 1 (Tctex1)
NM 009821	Runt related transcription factor 1 (Runx1)
NM 010149	Erythropoietin receptor (Rpor)
NM 011178	Proteinase 3 (Prtn3)
NM 013585	Proteosome (prosome, macrepain) subunit, beta type 9 (large multifunctional protease 2) (Psmb9)
NM 013814	UDP-*N*-acetyl-alpha-D-galactosamine:polypeptide *N*-acetylgalactosaminyltransferase 1 (Galnt1)
NM 013899	Translocase of inner mitochondrial membrane 13 homolog a (yeast) (Timm13a)
NM 018782	Calcitonin receptor-like (Calcrl)
NM 025570	Mitochondrial ribosomal protein L20 (Mrpl20)
NM 026479	DNA segment, Chr 11, ERATO Doi 416, expressed (D11Ertd416e)
NM 026965	Catechol-*O*-methyltransferase domain containing 1 (Comtd1)
NM 028906	Dipeptidylpeptidase 8 (Dpp8)
NM 030066	Armadillo repeat containing, X-linked 1 (Armcx1)
NM 133786	SMC4 structural maintenance of chromosomes 4-like 1 (yeast) (Smc4l1)
NM 148934	Gene trap ROSA b-geo 22 (Gtrgeo22)
NM 172562	Transcriptional adaptor 2 (ADA2 homolog, yeast)-like (Tada2l)
NM 173440	Nuclear receptor interacting protein 1 (Nrip1)
NM 177342	TAF5 RNA polymerase II, TATA box binding protein (TBP)-associated factor (TAF5)

CD34$^-$KSL cells in comparison with progenitor cells and differentiated cells [20]. Furthermore, gene expression profiles have been compared among different stem cells (SP CD34$^-$KSL HSCs, neural stem cells, and ES cells), with identification of genes expressed in common [21]. Both SP CD34$^-$KSL and CD34$^-$KSL cells are highly enriched for HSCs compared with fetal liver AA4.1$^+$KSL cells. However, the paucity of SP CD34$^-$KSL and CD34$^-$KSL cells in BM hampered approaches to expression profiling other than microarray analysis. Cyclopedic full-length cDNA sequencing projects, however, have provided us with an abundance of cDNA data for many kinds of organs, tissues, and cells, HSCs excepted [22]. To obtain a detailed gene expression profile of CD34$^-$KSL HSCs, we constructed a CD34$^-$KSL cDNA library and performed high-throughput sequencing. We then compared the resultant profile with that similarly obtained for another HSC fraction, SP Lin$^-$ cells.

The HSC libraries we constructed contained independent clones in numbers comparable with those in libraries made using similar methods (Figs. 1, 2) [23]. Successful subtraction of housekeeping genes in silico allowed us to focus on genes specific to hematopoietic cells (Fig. 4). As expected, most of the genes identified as in common among SCDb, CD34$^-$KSL, and SP Lin$^-$ libraries appeared to be HSC-specific by RT-PCR analysis, while the genes identified as in common only between CD34$^-$KSL and SP Lin$^-$ libraries contained those non-specific to HSCs (Fig. 5, Table 3). Contamination with genes that are not HSC-specific also indicated the limitations of our in silico subtraction approach (Table 3). Furthermore, representative HSC genes, including *GATA-2* and *Bmi1*, were identified in only one HSC library. This might be because too few clones were sequenced. However, this approach is suitable to identify novel transcripts or for profiling of genes with low expression levels, and indeed we could identify five novel genes that are HSC-specific in expression.

By GO assignment, we predicted functions of the identified genes (Fig. 3). Among genes assessed as encoding a membrane protein (CD34$^-$KSL: 122, SP Lin$^-$: 291, both populations: 118), we could use cell-function classifications to identify novel HSC cell surface marker candidates. These included cell adhesion, a biological process (CD34$^-$KSL: 10, SP Lin$^-$: 15, both populations: 7), and receptor activity, a molecular function (CD34$^-$KSL: 29, SP Lin$^-$: 72, both populations: 22). Indeed, among genes specific to CD34$^-$KSL and/or SP

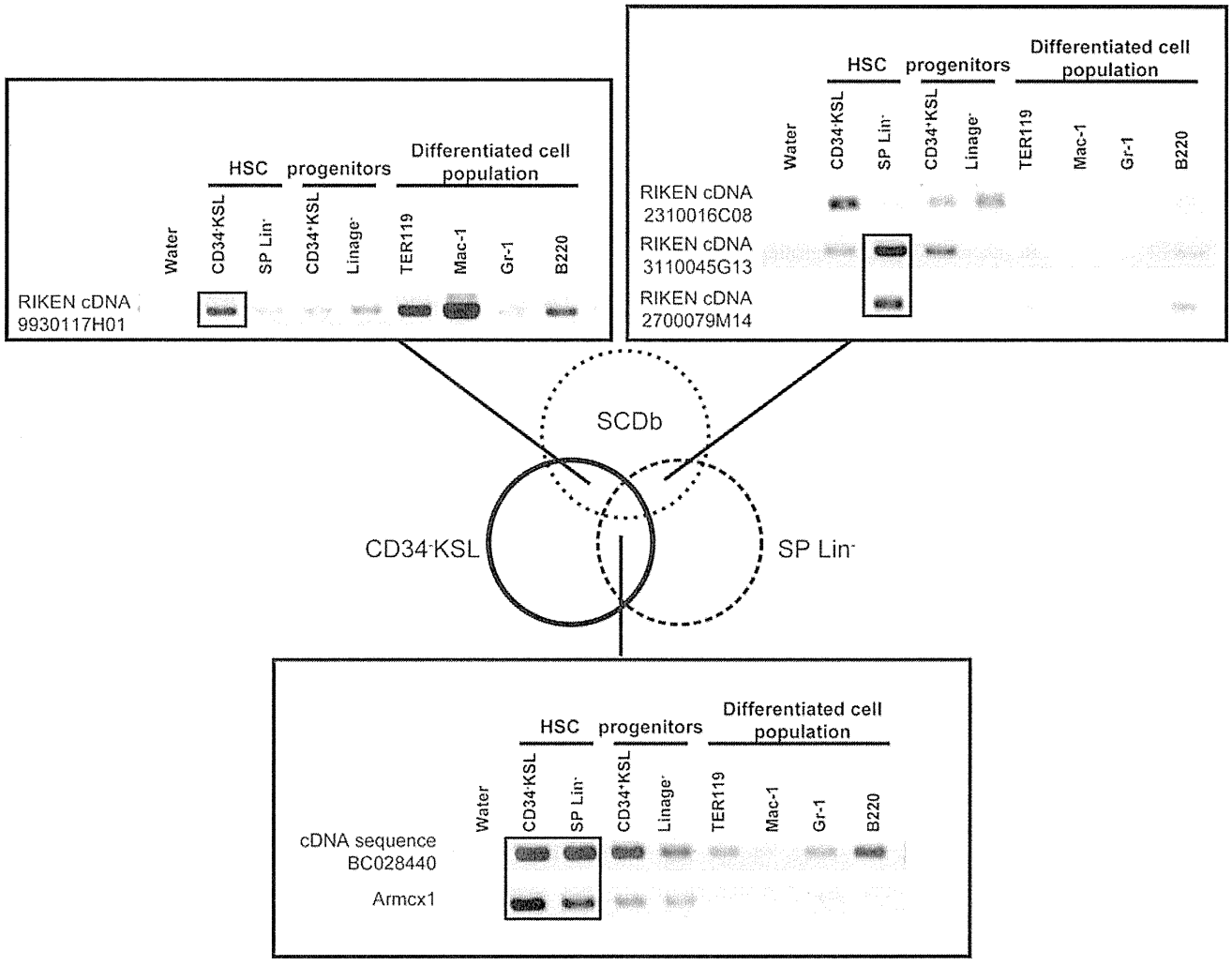

Fig. 5 Expression of identified genes. Expression of selected SCDb-listed genes shared between CD34$^-$KSL cells and SP Lin$^-$ cells and selected genes shared only between CD34$^-$KSL cells and SP Lin$^-$ cells was analyzed by RT-PCR. Cells analyzed are BM CD34$^-$KSL and SP Lin$^-$ HSCs, CD34$^+$KSL and Lineage marker$^-$ progenitors, TER119$^+$ erythroblasts, Mac-1$^+$ monocytes/macrophages, Gr-1$^+$ neutrophils, and B220$^+$ B cells

Lin$^-$ cells, the deduced amino acid sequence of RIKEN cDNA 9930117H01 contains both a putative signal peptide sequence and a transmembrane domain (Fig. 5). RIKEN cDNA 3110045G13 is similarly predicted to encode a cell surface transmembrane protein with extracellular EGF-like domains, and RIKEN cDNA 2700079M14 to encode a transmembrane protein with an extracellular immunoglobulin-like domain. To analyze expression specificities and functions of these putative cell surface proteins in HSCs would be intriguing. The GO profiling may help in understanding the molecular machineries operating in HSCs.

One of the most surprising results to emerge from mammalian cDNA sequencing projects is that thousands of mRNA-like non-coding RNAs are expressed, constituting at least 10% of poly(A)$^+$ RNAs [24, 25]. Non-coding RNAs are involved in the regulation of epigenetic functions, including chromatin structure and genome imprinting. Inactivation of the X chromosome by *Xist* RNA is a representative function of non-coding RNAs [26]. Some functions of non-coding RNAs in hematopoiesis have been reported [18, 19]. In most cases, however, the functions of these RNA molecules remain unclear. The biological significance of mRNA-like non-coding RNAs in HSCs in particular has not been clarified. We screened HSC clones for mRNA-like non-coding RNAs and identified 29 candidates. Our data suggest that some mRNA-like non-coding RNAs function in an HSC-specific manner. Understanding of the functions of HSC-specific mRNA-like non-coding RNAs would break open a new field of HSC biology.

By high-throughput sequencing analysis, we have added a number of genes to the list of HSC-specific genes and have identified HSC-specific putative mRNA-like non-

Table 3 Summary of the expression profiles of selected genes determined by RT-PCR

Gene/lineage	34^{-}KSL	SP-KSL	34^{+}KSL	Lin^{-}	Ter119	Mac-1	Gr-1	B220
Expression of all six genes identified as in common among SCDb, $CD34^{-}$KSL, and SP Lin^{-} libraries								
Gfi1b	+++	+++	++	+	++	−	−	±
3110045G13Rik	±	+++	+	−	−	−	−	−
Mfng	++	++	−	−	−	−	−	+
Rgs18	+++	±	+	++	−	±	−	−
Exosc2	±	±	±	±	±	−	−	±
Serpina3g	++	++	+	±	−	−	−	±
Expression of seven selected genes identified as in common only between $CD34^{-}$KSL and SP Lin^{-} libraries								
Armcx	+++	++	+	+	−	−	±	−
BC28440	+++	+++	++	+	±	−	±	+
D11Erf416e	+	+	±	++	−	−	−	±
1110019N10Rik	++	+	+	++	±	±	±	++
2810405O22Rik	++	++	++	++	++	±	++−	++
Bre	++	+++	+	+++	+++	+	+	+++
Calcrl	±	+	++	+	+++	±	−	±

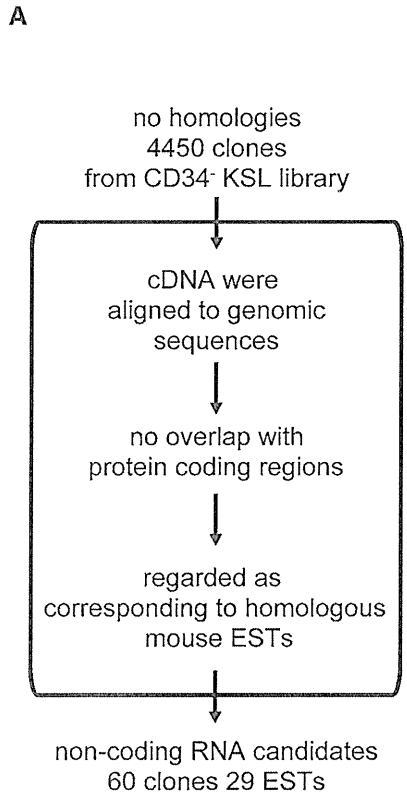

B

Chromosome No.	Clone No.	Accession No.
Chr 1	1	CN539228
Chr 1	1	AA596108
Chr 2	4	CX236158
Chr 3	4	CK795576
Chr 3	1	BE740716
Chr 4	1	CN697221
Chr 4	1	BB578787
Chr 4	2	CB598798
Chr 4	9	CB847565
Chr 4	1	BE534564
Chr 5	1	BQ892059
Chr 5	1	CX235980
Chr 5	1	BB683661
Chr 5	1	BP771729
Chr 6	1	CX220266
Chr 6	1	BX517570
Chr 6	8	CB849402
Chr 6	2	BU924501
Chr 8	1	BX528492
Chr 9	5	AU021499
Chr 11	1	CA881051
Chr 11	1	BQ567063
Chr 11	1	CK129343
Chr 11	1	CK377676
Chr 16	1	CA885675
Chr 17	2	BB661487
Chr 17	4	BM241006
Chr 17	1	BY722123
Chr 19	1	BE200491

Fig. 6 Identification of putative mRNA-like non-coding RNAs. **a** Scheme of the computational screening of non-coding RNA candidates. **b** List of non-coding RNA candidates. Chromosomal location, number of clones identified, and accession number of each candidate are indicated

coding RNAs. Further characterization of identified HSC-specific genes and their products, particularly with regard to their functional aspects in HSCs, will be highly helpful in elucidating the molecular mechanisms of HSC regulation.

References

1. Osawa M, Hanada K, Hamada H, Nakauchi H. Long-term lymphohematopoietic reconstitution by a single CD34-low/negative hematopoietic stem cell. Science. 1996;273:242–5.
2. Goodell MA, Brose K, Paradis G, Conner AS, Mulligan RC. Isolation and functional properties of murine hematopoietic stem cells that are replicating in vivo. J Exp Med. 1996;183:1797–806.
3. Zhou S, Schuetz JD, Bunting KD, Colapietro AM, Sampath J, Morris JJ, et al. The ABC transporter Bcrp1/ABCG2 is expressed in a wide variety of stem cells and is a molecular determinant of the side-population phenotype. Nat Med. 2001;7:1028–34.
4. Bertoncello I, Hodgson GS, Bradley TR. Multiparameter analysis of transplantable hemopoietic stem cells: I. The separation and enrichment of stem cells homing to marrow and spleen on the basis of rhodamine-123 fluorescence. Exp Hematol. 1985;13: 999–1006.
5. Spangrude GJ, Heimfeld S, Weissman IL. Purification and characterization of mouse hematopoietic stem cells. Science. 1988;241:58–62.
6. Uchida N, Weissman IL. Searching for hematopoietic stem cells: evidence that Thy-1.1lo Lin- Sca-1+ cells are the only stem cells in C57BL/Ka-Thy-1.1 bone marrow. J Exp Med. 1992;175: 175–84.
7. Jordan CT, Astle CM, Zawadzki J, Mackarehtschian K, Lemischka IR, Harrison DE. Long-term repopulating abilities of enriched fetal liver stem cells measured by competitive repopulation. Exp Hematol. 1995;23:1011–5.
8. Terskikh AV, Easterday MC, Li L, Hood L, Kornblum HI, Geschwind DH, et al. From hematopoiesis to neuropoiesis: evidence of overlapping genetic programs. Proc Natl Acad Sci USA. 2001;98:7934–9.
9. Park IK, He Y, Lin F, Laerum OD, Tian Q, Bumgarner R, et al. Differential gene expression profiling of adult murine hematopoietic stem cells. Blood. 2002;99:488–98.
10. Venezia TA, Merchant AA, Ramos CA, Whitehouse NL, Young AS, Shaw CA, et al. Molecular signatures of proliferation and quiescence in hematopoietic stem cells. PLoS Biol. 2004;2(10): e301. doi:10.1371/journal.pbio.0020301.
11. Phillips RL, Ernst RE, Brunk B, Ivanova N, Mahan MA, Deanehan JK, et al. The genetic program of hematopoietic stem cells. Science. 2000;288:1635–40.
12. Ivanova NB, Dimos JT, Schaniel C, Hackney JA, Moore KA, Lemischka IR. A stem cell molecular signature. Science. 2002;298:601–4.
13. Chambers SM, Boles NC, Lin KY, Tierney MP, Bowman TV, Bradfute SB, et al. Hematopoietic fingerprints: an expression database of stem cells and their progeny. Cell Stem Cell. 2007;1:578–91.
14. Kitamura T, Koshino Y, Shibata F, Oki T, Nakajima H, Nosaka T, et al. Retrovirus-mediated gene transfer and expression cloning: powerful tools in functional genomics. Exp Hematol. 2003;31:1007–14.
15. Altschul SF, Gish W, Miller W, Myers EW, Lipman DJ. Basic local alignment search tool. J Mol Biol. 1990;215:403–10.
16. Ashburner M, Ball CA, Blake JA, Botstein D, Butler H, Cherry JM, et al. Gene ontology: tool for the unification of biology. The gene ontology consortium. Nat Genet. 2000;25:25–9.
17. Osawa M, Yamaguchi T, Nakamura Y, Kaneko S, Onodera M, Sawada K, et al. Erythroid expansion mediated by the Gfi-1B zinc finger protein: role in normal hematopoiesis. Blood. 2002;100:2769–77.
18. Chen CZ, Li L, Lodish HF, Bartel DP. MicroRNAs modulate hematopoietic lineage differentiation. Science. 2004;303:83–6.
19. Wagner LA, Christensen CJ, Dunn DM, Spangrude GJ, Georgelas A, Kelley L, et al. EGO, a novel, noncoding RNA gene, regulates eosinophil granule protein transcript expression. Blood. 2007;109:5191–8.
20. Akashi K, He X, Chen J, Iwasaki H, Niu C, Steenhard B, et al. Transcriptional accessibility for genes of multiple tissues and hematopoietic lineages is hierarchically controlled during early hematopoiesis. Blood. 2003;101:383–9.
21. Ramalho-Santos M, Yoon S, Matsuzaki Y, Mulligan RC, Melton DA. "Stemness": transcriptional profiling of embryonic and adult stem cells. Science. 2002;298:597–600.
22. Okazaki Y, Furuno M, Kasukawa T, Adachi J, Bono H, Kondo S, et al. Analysis of the mouse transcriptome based on functional annotation of 60, 770 full-length cDNAs. Nature. 2002;420: 563–73.
23. Numata K, Kanai A, Saito R, Kondo S, Adachi J, Wilming KG, et al. Identification of putative noncoding RNAs among the RIKEN mouse full-length cDNA collection. Genome Res. 2003;13:1301–6.
24. Simin K, Scuderi A, Reamey J, Dunn S, Weiss R, Metherall JE, et al. Profiling patterned transcripts in Drosophila embryos. Genome Res. 2002;12:1040–7.
25. Barciszewski J, Vrdmann VA. Noncoding RNAs: molecular biology and molecular medicine. Georgetown, TX/New York, NY. Landes Bioscience/Eurekah.com; Kluwer Academic/Plenum Publishers; 2003.
26. Brockdorff N, Ashworth A, Kay GF, Cooper P, Smith S, McCabe VM, et al. Conservation of position and exclusive expression of mouse Xist from the inactive X chromosome. Nature. 1991;351: 329–31.

Identification of cancer stem cells in a Tax-transgenic (Tax-Tg) mouse model of adult T-cell leukemia/lymphoma

*Jumpei Yamazaki,[1,2] *Takuo Mizukami,[1] Kazuya Takizawa,[1] Madoka Kuramitsu,[1] Haruka Momose,[1] Atsuko Masumi,[1] Yasushi Ami,[3] Hideki Hasegawa,[4] William W. Hall,[5] Hajime Tsujimoto,[2] Isao Hamaguchi,[1] and Kazunari Yamaguchi[1]

[1]Department of Safety Research on Blood and Biologics, National Institute of Infectious Diseases, Tokyo, Japan; [2]Veterinary Internal Medicine, University of Tokyo, Tokyo, Japan; Departments of [3]Animal Science and [4]Pathology, National Institute of Infectious Diseases, Tokyo, Japan; and [5]Centre for Research in Infectious Diseases, School of Medicine & Medical Science, University College Dublin, Dublin, Republic of Ireland

Adult T-cell leukemia/lymphoma (ATL) is a malignant lymphoproliferative disorder caused by HTLV-I infection. In ATL, chemotherapeutic responses are generally poor, which has suggested the existence of chemotherapy-resistant cancer stem cells (CSCs). To identify CSC candidates in ATL, we have focused on a Tax transgenic mouse (Tax-Tg) model, which reproduces ATL-like disease both in Tax-Tg animals and also after transfer of Tax-Tg splenic lymphomatous cells (SLCs) to nonobese diabetic/severe combined immunodeficiency (NOD/SCID) mice. Using a limiting dilution transplantation, it was estimated that one CSC existed per 10^4 SLCs (0.01%). In agreement with this, we have successfully identified candidate CSCs in a side population (0.06%), which overlapped with a minor population of $CD38^-/CD71^-/CD117^+$ cells (0.03%). Whereas lymphoma did not develop after transplantation of 10^2 SLCs, 10^2 CSCs could consistently regenerate the original lymphoma. In addition, lymphoma and CSCs could also be demonstrated in the bone marrow and $CD117^+$ CSCs were observed in both osteoblastic and vascular niches. In the CSCs, *Tax*, *Notch1*, and *Bmi1* expression was down-regulated, suggesting that the CSCs were derived from Pro-T cells or early hematopoietic progenitor cells. Taken together, our data demonstrate that CSCs certainly exist and have the potential to regenerate lymphoma in our mouse model. (Blood. 2009;114:2709-2720)

Introduction

Adult T-cell leukemia-lymphoma (ATL) is an aggressive and clonal lymphoproliferative disorder of mature T cells caused by infection with human T-lymphotropic virus type I (HTLV-1).[1] An estimated 10 million to 20 million people are infected with HTLV-1 globally, and infection is endemic in southwestern Japan, Africa, the Caribbean basin, and South America.[2] Although the majority of infected persons remain clinically asymptomatic, approximately 6.6% of males and 2.1% of females will develop ATL. In Japan, 1.2 million persons are infected with HTLV-1, and 800 to 1000 new ATL cases develop each year. ATL has been divided into 4 subtypes: chronic, smoldering, acute, and lymphoma-type.[3] Acute and lymphoma-type have an aggressive clinical course with lymphadenopathy, hepatosplenomegaly, visceral invasion by malignant cells, and the appearance of leukemic cells with multilobulated nuclei termed "flower cells" in peripheral blood. The most common cell phenotype in ATL is $CD2^+$, $CD3^+$, $CD4^+$, $CD8^-$, and $CD25^+$. Other phenotypes, which include $CD4^-/CD8^-$ double-negative (DN), $CD8^+$, and $CD4^+/CD8^+$ double-positive, occur more rarely.[4] FOXP3 (forkhead box P3) expression, which is predominantly expressed in $CD4^+/CD25^+$ regulatory T cells (Tregs), has also been detected in some ATL cases, suggesting that disease may originate in Treg cells.[5] In addition, HTLV-I can also infect human hematopoietic progenitor cells and immature thymocytes, which would also account for the range of phenotypes observed.[6]

Studies have shown that initiation of oncogenesis is triggered by the viral Tax protein. Tax interacts with the nuclear factor-κB (NF-κB)–Rel signaling complex and activates NF-κB, which results in the up-regulation of various cytokines and their receptor genes, and alterations in cell signaling and cell-cycle regulation.[7] Recent studies have clearly demonstrated the oncogenic properties of Tax in vivo. Specifically, transgenic animals with Tax expression restricted to developing thymocytes developed an ATL-like phenotype and leukemogenesis developed in both immature[8] and mature T cells.[9] The treatment of ATL is unsatisfactory. Various combination chemotherapy regimens have produced poor outcomes; however, intensive induction therapy (interferon-α and zidovudine) has produced significant complete remission rates in certain cases.[10,11] Unfortunately, most patients relapse, and this has been considered to be the result of the existence of cancer stem cells (CSCs) similar to what has been described both in other types of leukemia and solid tumors. Specifically, CSCs have been identified in malignancies of both hematopoietic origin[12,13] and in breast, brain, prostate, colon, and pancreatic carcinomas.[14] CSCs have the potential to self-renew, develop inherent drug-resistance, and can regenerate the original tumors when transplanted into severe combined immunocompromised nonobese diabetic/severe combined immunodeficiency (NOD/SCID) mice.[15] As a consequence, CSCs are considered important targets for anticancer therapy.[16]

To identify and confirm the existence of CSCs in ATL, we have focused our initial studies on an HTLV-Tax transgenic mouse (Tax-Tg) model,[8] where transgene expression was controlled by the LCK promoter, which limits transgene expression to developing thymocytes. The clinical, pathologic, and immunologic features observed in this Tax-Tg model are similar to those observed in the

Submitted August 17, 2008; accepted May 28, 2009. Prepublished online as *Blood* First Edition paper, July 7, 2009; DOI 10.1182/blood-2008-08-174425.

An Inside *Blood* analysis of this article appears at the front of this issue.

*J.Y. and T.M. contributed equally to this study.

The publication costs of this article were defrayed in part by page charge payment. Therefore, and solely to indicate this fact, this article is hereby marked "advertisement" in accordance with 18 USC section 1734.

aggressive forms of human ATL. Lymphoma and leukemia develop at 10 to 23 months, which is equivalent to human disease (20-60 years) and is characterized by the widespread distribution of lymphomatous cells in various organs and the presence of flower cells in peripheral blood. Lymphomatous cells displayed a $CD4^-CD8^-$ DN phenotype. In addition, lymphomas could be regenerated in NOD/SCID mice after transplantation of Tax-Tg splenic lymphomatous cells. In this study, we have successfully identified candidate CSCs using xenografting into NOD/SCID mouse and flow cytometric analysis. Specifically, we identified CSCs in a side population (SP; 0.06%), which overlapped with a minor population of $CD38^-/CD71^-/CD117^+$ cells (0.03%). Using the NOD/SCID transplantation assay, we found that 10^2 CSCs could regenerate the original lymphoma. This is first report describing a CSC candidate in an ATL model, and we think that similar studies will inform and may ultimately allow the identification of CSCs in human disease.

Methods

Animal models of ATL

Animal experiments were approved by the Animal Care and Use Committee of the National Institute of Infectious Disease, Tokyo, Japan. For transplantation studies, we obtained NOD/SCID mice (NOD.CB17-Prkdc^{scid}/J) 6 to 12 weeks of age from The Jackson Laboratory, and these were housed under constant temperature and light.

Transplantation assays

ATL-like lymphoma and leukemia was first established in NOD/SCID mice by intraperitoneal injection of 10^5 frozen stock Tax transgenic (Tax-Tg) splenic lymphomatous cells (SLCs). After 40 days, ATL-like lymphoma developed in the NOD/SCID mouse spleen, and SLCs could regenerate the original ATL-like lymphoma when further injected. Using this NOD/SCID mouse transplantation system, SLCs could be serially passed as required. We used 4th-passage frozen stocked SLCs for the serial transplantation studies. We performed 3 consecutive serial transplantations by intraperitoneal injection of 10^5 SLCs (first transplantation [n = 12], second transplantation [n = 5], third transplantation [n = 7]). We also performed limiting dilution assays by intraperitoneal injection of 10^6 (n = 5), 10^5 (n = 4), 10^4 (n = 3), 10^3 (n = 5), and 10^2 (n = 7) of freshly isolated SLCs. To evaluate the lymphoma-forming ability of CSC candidates, we also transplanted 10^2 CSCs ($CD38^-/CD71^-/CD117^+$; n = 9), non-CSC fraction ($CD38^+/CD71^+/CD117^-$; n = 11), and SLCs (n = 11) into NOD/SCID mice.

Flow cytometry and SP analysis

To identify candidate CSCs in the SLCs, we performed SP cell analysis. SLCs were suspended in Hanks balanced salt solution medium (Invitrogen) containing 2% fetal bovine serum, 10 mM N-2-hydroxyethylpiperazine-N′-2-ethanesulfonic acid buffer (Invitrogen), and incubated with Hoechst 33342 dye (2.5 μg/mL, Invitrogen, H-3570) with or without verapamil (Sigma-Aldrich) at 37°C for 60 minutes, according to the method outlined by Goodell et al.[17] After staining with or without Hoechst 33342, the cells were stained with phycoerythrin (PE) anti–mouse/rat Foxp3 (clone FJK-16s), PE anti–mouse CD3e (145-2C11), PE anti–mouse CD8 (53-6.7), PE anti–mouse CD127 (clone A7R34), PE anti–mouse CD38 (clone 90), fluorescein isothiocyanate (FITC) anti–mouse Sca-1 (clone D7), FITC anti–mouse CD2 (RM2-5), FITC anti–mouse CD4 (RM4-5), FITC anti–mouse CD123 (clone 5B11), FITC anti–mouse CD24 (clone 30-F1), FITC anti–mouse CD71 (clone R17217), and allophycocyanin (APC) anti–mouse CD25 (clone PC61.5), APC anti–mouse CD133 (clone 13A4), APC anti–mouse CD117(clone ACK2), APC anti–mouse CD25 (PC61.5), and purified anti–mouse CD44 (IM7) at 4°C for 30 minutes and then counterstained with 2 μg/mL propidium iodide (BD Biosciences). All antibodies were obtained from eBioscience. We performed flow-cytometric analysis and cell sorting using JSAN (Bay Bioscience) with 350-nm UV laser for SP analysis. Cytospin preparations of the sorted cells were prepared and subjected to Wright/Giemsa staining.

Histologic preparation and periodic acid-Schiff–hematoxylin staining

NOD/SCID mouse spleen, bone marrow (BM), liver, lung, lymph node, and epidermal tissues were harvested and fixed in Bouin solution (Sigma-Aldrich) or 4% (wt/vol) paraformaldehyde in phosphate-buffered saline (pH 7.5) at 4°C for 24 hours. After fixation, samples were dehydrated in a graded ethanol series and cleared in xylene, and then embedded in paraffin; 4-μm semithin sections were prepared using a carbon steel blade (Feather Safety Razor Co) by microtome (Yamato Kouki). Tissue sections were mounted on super-frosted glass slides coated with methyl-amino-silane (Matsunami Glass). To identify periodic acid-Schiff (PAS)–positive ATL leukemia/lymphoma[18] in spleen, we performed PAS-hematoxylin staining as previously described.[19] Histologic images were aqquired using a NikonEclipse E1000 microscope equipped with 10×/0.30, 20×/0.50, 40×/0.75, and 100×/1.30 NA objective lenses. Images were captured with a Nikon DXM 1200F digital camera.

Immunohistochemistry

Anti–mouse CD3 antibody (ab5690; Abcam), anti–mouse CD44 (IM7; BioLegend), anti–mouse/human CD117 (C-19; Santa Cruz Biotechnology), and anti–mouse CD4 (RM4-5; eBioscience) were used as primary antibodies, and biotinylated goat anti–rat IgG-B (SC-2041, Santa Cruz Biotechnology) and biotinylated goat anti–rabbit IgG-B (SC-2040, Santa Cruz Biotechnology) were used as secondary antibodies. Staining was carried out as previously described.[20] Briefly, after blocking with 3% bovine serum albumin (BSA) in phosphate-buffered saline, sections (4-μm thick) were incubated with anti-CD3, -CD4, -CD44, and -CD117 antibody (each diluted 1:200) at 4°C overnight. Signals were detected using a Vectastain ABC Elite Kit (Vector Laboratories), and nuclei were stained with Gill III-hematoxylin.

Quantitative analysis of gene expression

Poly (A)+ RNAs were extracted from 5×10^3 candidate CSCs ($CD38^-/CD71^-/CD117^+$) and non-CSCs ($CD38^+/CD71^+/CD117^-$) using a Micro-Fast Track 2.0 Kit (Invitrogen), and cDNAs were prepared using SMART polymerase chain reaction (PCR) cDNA synthesis kits (Clontech) as previously described.[20] Real-time PCR reactions were performed using SYBR PreMix ExTaq (Takara Shuzo) and a Light Cycler (Roche Diagnostics). The primer pairs used in this study were *Notch1* (5′-CGTGGTCTTCAAGCGTGATG-3′ and 5′-AGCTCTTCCTCGTGGCCATA-3′), *CD44* (5′-AGCTGACGAGACCCGGAAT-3′ and 5′-CGTAGGCACTACACCCCAATC-3′), *Rex1* (5′-TGTGCTGCCTCCAAGTGTTG-3′ and 5′-ATCCGCAAACACCTGCTTTT-3′), and *N-cadherin* (5′-CACAGCCACAGCCGTCATC-3′ and 5′-GCAGTAAACTCTGGAGGATTGTCA-3′) and for *Tax*,[8] *CD117*, *Bmi1*, *SCL/tal-1*, and *β-actin* as previously described.[20] *β-Actin* was used as an internal control. Real-time PCR was carried out using 40 cycles at 94.0°C for 1 minute, 60°C for 25 seconds (2-step). Amplification of predicted fragments was confirmed by melt-curve analysis and gel electrophoresis. To determine the relative amounts of product, we used the comparative threshold cycle method, according to the manufacturer's instructions (Roche Diagnostics). Expression levels are reported relative to mouse *β-actin*.

Genomic DNA isolation and PCR assays for Tax transgene integration mapping

Genomic DNA was extracted from 5×10^6 splenic and BM mononuclear cells using the DNeasy Blood & Tissue Kit system (QIAGEN). Cells were isolated from NOD/SCID mice with or without transplantation of Tax-Tg-derived SLCs. All genomic DNAs were treated with RNase A (100 mg/mL).

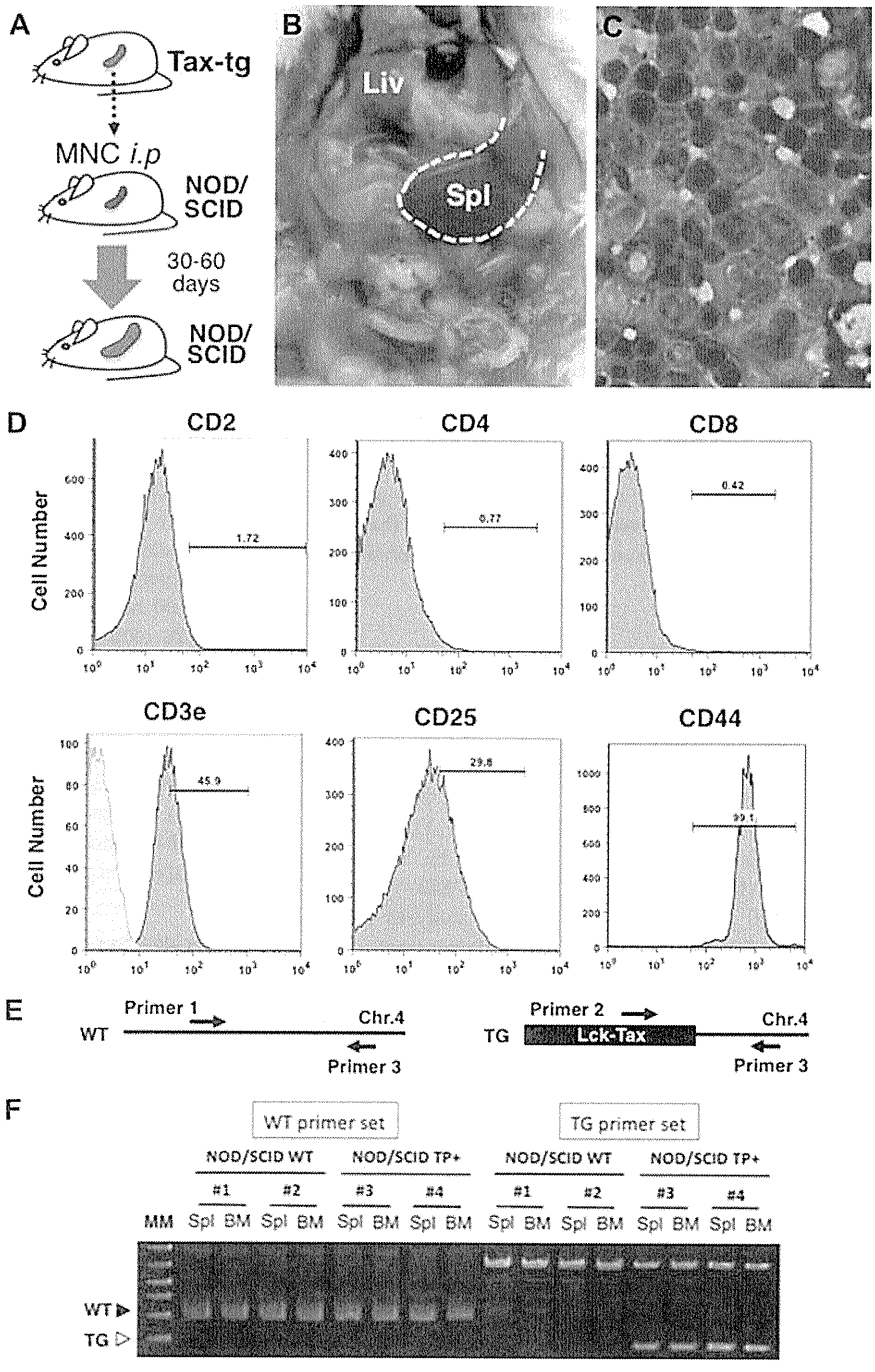

Figure 1. Transplantation of Tax-Tg mouse-derived splenic mononuclear cells to NOD/SCID mice. (A) Experimental design of the transplantation assay. (B) Remarkable splenomegaly was observed in the lymphoma-reconstituted NOD/SCID mouse. Spl indicates spleen; and Liv, liver. The dotted line shows the outline of the enlarged spleen. (C) Cytospin analysis of spleen cells isolated from reconstituted lymphoma in the NOD/SCID mouse. The spleen was filled with ATL-like lymphomatous cells. (D) Surface marker analysis of lymphomatous cells from spleen. These had the identical phenotype of lymphomatous cell reconstituted by Tax-Tg–derived splenic mononuclear cells: $CD2^-$, $CD4^-$, $CD8^-$, cytoplasmic $CD3^+$, and surface $CD25^+$ and $CD44^+$. (E) Schematic representation of the PCR assay to identify and confirm the Tax transgenic integration site. Lck-Tax transgenes were tandemly inserted on the chromosome 4 (Chr.4) in the original transgenic animals. (F) Genotyping of mononuclear cells in the spleen and BM. WT PCR product (300 bp) was detected in both the normal and CSC-transplanted NOD/SCID spleen and BM. However, Tax-Tg (TG) PCR products identifying the expected integration site of the transgene (200 bp) were detected only in the reconstituted ATL-like lymphomatous cells in spleen and BM. TP+ indicates transplantation.

PCR primers were constructed based on the integration site of Tax gene on chromosome 4 in the Tax-Tg mouse model.[8] The primers used to detect the Tax-Tg or wild-type (WT) NOD/SCID mouse derived genomic DNA were NOD/SCID mouse (5′-TGT TGC ATA CAG GAA GCC CA-3′ and 5′-GCG GTA CAG TGT GTG CTT TGA G-3′) and Tax-Tg (5′-GAC ACA GCA TAG GCT ACC TGG C-3′ and 5′-GCG GTA CAG TGT GTG CTT TGA G-3′; Figure 1E). PCR reactions were performed using ExTaq (Takara Shuzo) and a Thermal Cycler (Bio-Rad). The PCR was carried out using 95°C for 2 minutes, 40 cycles at 94.0°C for 30 seconds, 58°C for 30 seconds, and 72°C for 30 seconds. The PCR products were analyzed by electrophoresis on 2% agarose gels.

Data analysis

Significant differences were calculated using the Student *t* test for gene expression analysis. Statistical analyses were performed using GraphPad Prism (Version 5, GraphPad Software) and Excel 2008 (Microsoft Japan).

Results

Lymphoma/leukemia regenerative activity in the Tax-Tg mouse and SLCs

Hasegawa et al reported that Tax-Tg SLCs could regenerate ATL-like lymphoma when transplanted into NOD/SCID mice and that Tax-Tg SLCs had the potential to regenerate the original lymphoma when further transplanted in NOD/SCID mice.[8] To assess the stem cell potential within the SLCs, we performed serial transplantation experiments by intraperitoneal injections of frozen stocked 4th-passed 10^5 SLCs into NOD/SCID mice (Figure 1A). SLCs could regenerate original lymphoma and leukemia in the first transplantation (12 of 12 animals) with the development of marked

splenomegaly (Figure 1B-C) and BM involvement resulting from infiltration of malignant cells. The phenotypes of the SLCs were similar to the original tumors in Tax-Tg animals. Surface staining for CD2, CD4, and CD8 was negative, but cytoplasmic CD3 and surface CD25 and CD44 were positive in the SLCs (Figure 1D). SLCs could regenerate original lymphoma and leukemia after second (5 of 5 animals) and third transplantation (6 of 7 animals) by day 40.

To confirm that the SLCs were derived from the original leukemic cells, we performed PCR analysis to confirm the Tax transgenic integration site. In the Tax-Tg model, the transgene was found to be integrated in the A9 region of chromosome 4. PCR analysis with amplification across the integration site demonstrated that this was identical in the lymphomatous cells arising in both spleen and BM (Figure 1E-F), confirming that they were derived from the original leukemic cells and that variant populations had not arisen nor were selected. These studies provided functional evidence for self-renewal and supported the existence of CSCs, which have leukemia/lymphoma regenerative potential, within the SLCs.

Identification of CSCs in SLCs by surface marker analysis

It has been suggested that CSCs are a small and minor population in both leukemias[12,13] and solid tumors.[14] To identify the candidate CSC populations in SLCs, we performed detailed cell surface marker analysis, to investigate phenotypic expression patterns previously observed in Tregs (CD25, CD127, FoxP3), hematopoietic stem cells (HSCs; CD117, CD34, CD38, Sca-1, c-kit), and markers previously identified in other CSCs (CD71, CD123, CD24, CD90, CD133). Surface marker analyses are shown in Figure 2A through D. Expression patterns were divided into 4 profiles: partial and low expression; CD127, CD117, CD123, FoxP3, CD133, CD90, and CD34 (Figure 2B); heterogeneous expression; CD71 and CD25 (Figure 2C); and major expression; CD38, CD24, and Sca-1 (Figure 2D).

Certain cases of human ATL are thought to originate from Tregs, which express CD4, $CD25^{int\text{-}hi}$, FOXP3,[21] and CD127.[22] Whereas Foxp3 expression was not detected (0.03%) in the SLCs, CD25 expression was heterogeneously detected (64.5%) and CD127 expression was detected at low levels (1.17%; Figure 2B-C). Recent studies have shown that leukemia stem cells can share HSC properties ($CD34^+/CD38^-$ cells), and it could also be shown that these could regenerate the original disease in NOD/SCID mice.[23] In the mouse, HSCs are enriched in $CD34^-/c\text{-}kit^+/Sca\text{-}1^+/Lineage^-$ cell population.[24] CD34 and CD117 (c-kit) expression in the SLCs was partially detected (0.63% and 0.56%). CD38 and Sca-1 highly expressed at 94.3% and 89.9%, respectively (Figure 2B,D). We also examined expression of CD123 (IL-3Ra), which is a well-established marker for leukemia stem cells,[12] CD133, which is a common CSC marker found in brain,[25] and colon cancer,[26] CD24, which has been identified in prostate CSCs,[27] and CD90, which is associated with CSCs in non-small-cell lung carcinoma.[28] In the SLCs, expression of CD71 and CD24 were 52.2% and 92.7%, respectively. In contrast, the expression of CD123, CD90, and CD133 was only detected at low levels, 0.13%, 0.89%, and 0.3%, respectively (Figure 2B-D).

Next, we performed multiple stainings for the identification of small populations within the SLCs (Table 1), and we successfully identified such a population, which was $CD38^-/CD71^-$. With a combination of CD117, we successfully confirmed the existence of a minor population (0.03%), which was $CD38^-/CD71^-/CD117^+$ (Figure 2E). In contrast, $CD38^-/CD71^-/CD133^+$ cells were not detected in SLCs (0%).

Identification of candidate CSCs for functional studies

Recent studies have shown that SPs are enriched for CSCs in various types of malignancies.[29] The SP phenotype is based on the ability of the cells to efficiently reflux the Hoechst 33342 fluorescent staining dye through the multidrug ABC transporter (ABCG2), and this property allows the isolation of the cells using flow cytometry. It is also considered that efflux efficiency in CSCs correlates with anticancer drug resistance and recurrence of disease after chemotherapy. To identify candidate CSCs, we investigated the SPs by evaluating efficient efflux of Hoechst 33342 dye in the SLCs. We successfully identified a small population (0.06%) corresponding to SP cells in the SLCs (Figure 3A); correspondingly, the SP fraction disappeared with treatment with the ABC transporter inhibitor verapamil. To further characterize the SP cells, we performed combination SP and surface marker analysis, and it could be shown that more than 50% of $CD38^-/CD71^-/CD117^+$ cells overlapped with the SP fraction in the SLCs (Figure 3B), suggesting that the CSC candidate(s) were associated with these populations.

The candidate CSC cells were also sorted for morphologic studies (Figure 3C). Isolated $CD38^-/CD71^-/CD117^+$ cells were blastoid cells and had scanty cytoplasm with no granules (Figure 3D). In contrast, $CD38^+/CD71^+/CD117^-$ cells were slightly larger and lymphocyte-like with dispersed chromatin and an irregularly shaped and prominent nucleus (Figure 3E).

In vivo lymphoma reconstitution assay of candidate CSCs

We performed transplantation analysis to assess the functionality of the candidate CSCs using the NOD/SCID mouse model. In initial studies, we performed limiting dilution analysis to estimate the frequency of the CSCs in the SLCs. We transplanted 10^6, 10^5, 10^4, 10^3, and 10^2 SLCs into NOD/SCID mice. It has been previously demonstrated that 10^5 SLCs could regenerate original leukemia and lymphoma observed in the Tax-Tg mice,[8] and this was evident by marked splenomegaly and confirmed by cytology at 40 days after transplantation. Spleen weights were approximately 10- to 20-fold larger than non-treated NOD/SCID mouse spleen (data not shown). In addition to the development of lymphoma, ascites also developed in the NOD/SCID mice. Using these criteria, we evaluated the lymphoma-regenerative activity in the candidate CSC and non-CSC fractions (Table 2). Whereas 10^2 SLCs could not regenerate original lymphoma and leukemia (0%) in the NOD/SCID mouse, 10^4 SLCs could, as expected, regenerate the original lymphoma and leukemia in all animals (100%). Lymphoma and leukemia after transplantation of 10^3 SLCs developed in 20% of animals. These results suggested that one CSC existed in 10^4 SLCs (0.01%), and indeed this frequency estimate was consistent with our surface marker and SP analysis studies.

We then isolated CSCs from SLCs, and 10^2 CSCs were transplanted into NOD/SCID mouse. At 40 days after transplantation, lymphoma and leukemia formation was not observed in 6 of the CSC transplanted NOD/SCID mice examined. However, at 60 days after transplantation, ATL-like lymphoma was observed in all 9 of the 9 CSC-injected NOD/SCID mice. All developed typical splenomegaly (Figure 4A-B) and ascites (Figure 4C). Total spleen

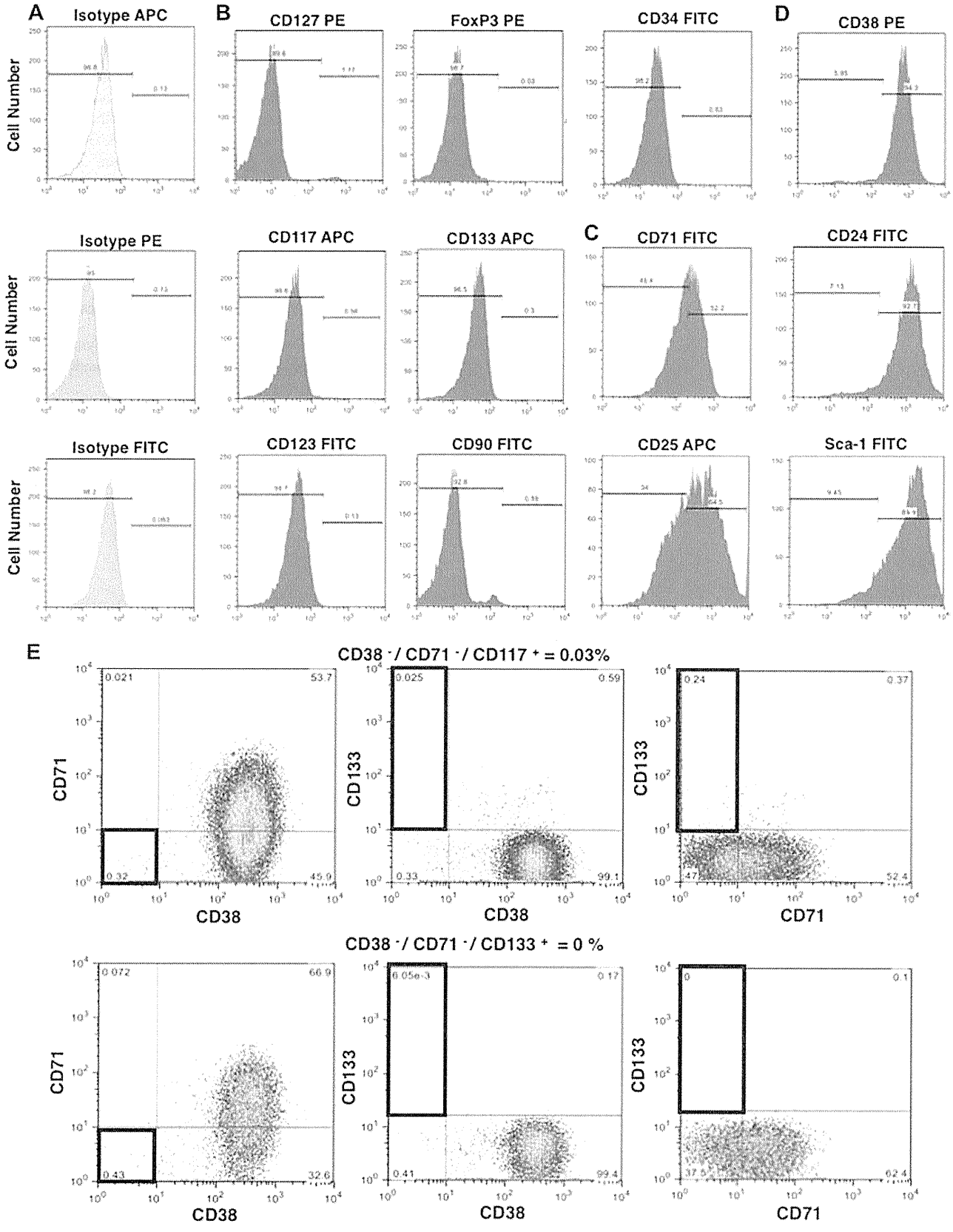

Figure 2. Flow cytometric analysis of NOD/SCID repopulating ATL-like lymphoma cells. Lymphoma and leukemia were generated in NOD/SCID mice by the transplantation of frozen stocked 4th-passage Tax-Tg SLCs. SLCs were isolated from spleen. (A) Histograms of isotype APC, PE, and FITC markers as controls. Expression profiles were divided into 4 patterns: partial and low, heterogeneous, and major types. (B) Partial and low expression: CD127, CD117, CD123, FoxP3, CD133, CD90, and CD34 are expressed at low levels in SLCs. (C) Heterogeneous expression: CD71 and CD25 are heterogeneously expressed in SLCs. (D) Major: CD38, CD24, and Sca-1 are highly expressed in SLCs. The percentage of individual subpopulations was determined according to isotype control in each assay. Dead cells were gated out by propidium iodide. (E) Triple-staining analysis with CD38, CD71, and CD117 or CD133 in the SLCs. $CD38^-/CD71^-/CD117^+$ cells were 0.03% and $CD38^-/CD71^-/CD133^+$ cells were 0% of total SLCs.